Bifurcation cascades at border collisions: characteristic scaling and their role in a yeast cell cycle

M R Jeffrey and H Dankowicz

January 8, 2014

1 Introduction

Piecewise smooth maps are a subject of increasing scientific interest, particularly as a description of global dynamics in piecewise smooth flows. A piecewise smooth map, or a "map with a gap" [**?**], is defined smoothly only over portions of its domain, with discontinuities in between. When a map is derived as a stroboscopic snapshot of a flow, discontinuities are often the result of tangential contact, known as *grazing*, between the flow and a hypersurface at which a discontinuity is introduced. In the neighbourhood of grazing, small perturbations cause the flow to either intersect the discontinuity, or miss it, creating a corresponding discontinuity in the global dynamics. Well known examples of discontinuous maps pertaining to grazing arise in the mechanics of impact [] and fluid layer contact []. Piecewise smooth maps have been studied in their own right, for example in models of heart arrhythmia [], neuron firing [], and electrical power converters []; see [**?**] for a review.

In the last two decades, grazing has taken on an important role in the analysis of discontinuity-induced bifurcations []. The local quadratic curvature of a flow that is generic near grazing leads, under certain conditions, to a square root map on one side of a discontinuity. As a result, square root maps are among the most studied of the piecewise smooth maps []. Interest has also focussed on period adding cascades [**?**, **?**, **?**, **?**], that is, sequences of periodic orbit bifurcations in which periodicity can increase by arbitrary integer values. The most general results pertain to cascades as a route to chaos [**?**, **?**], or assuming linearity of the map either side of the discontinuity [**?**, **?**, **?**], and are often restricted to maps in one dimension.

The cascade presented in this paper will differ from previous studies in three important aspects. Firstly, no chaotic dynamics is involved. Instead, the organising feature appears to be the instantaneous coexistence of two orbits, one of which crosses the discontinuity surface twice, the other which cross the discontinuity infinitely many times and reaches a grazing point in positive and negative time. Secondly, nonlinearity to the map will be shown to have striking implications for the cascade phenomenon, revealing that the cascade need not be 'discontinuity-induced' in the usual sense, since the bifurcation that causes the cascade may take place away from the discontinuity.

Thirdly, the cascade will be shown to be well described by a one dimensional piecewise smooth map, and yet describes accurately certain cascades of periodic orbits observed in simulations of the budding yeast cell life cycle [**?**]. In fact, observations of cascades in the model of the cell life cycle in [] were the motivation of the present study. The cell model is based upon experimentally observed processes of eukaryotic cell growth. The growth cycle involves exponential increase of cell mass, accompanied by variations in activator and inhibitor protein concentrations, modeled by a set of coupled nonlinear ordinary differential equations. Once per cycle a mitosis (cell division) event divides the cell mass in two, triggered when the concentration of a particular protein – cyclin B –

falls below a critical value. A universal scaling will be derived from the one-dimensional map, and is found to accurately describe cascades in the full model, both qualitatively and quantitatively.

In the biological model, a period p orbit represents a cycle of cell growth over which the mass at division oscillates between p different values. For a range of parameters there exists a cell cycle of period two, and this orbit is stable (attracting). At a critical parameter the periodic orbit disappears, either by grazing the mass division threshold, or by colliding with an unstable period two orbit in a saddle-node bifurcation. In either case, the disappearance is accompanied by the creation of a new attractor that can be described as a grazing orbit of infinite period: a closed orbit that visits infinitely many different masses at division, and visits the same grazing point forward and backwards in time. Nearby in parameter space this orbit gives way to periodic orbits of arbitrarily high period, whose period cascades down through the odd integers. The cascade occurs for physically reasonable parameters, and could in principle be observed by clustering of cell masses in populations of cells.

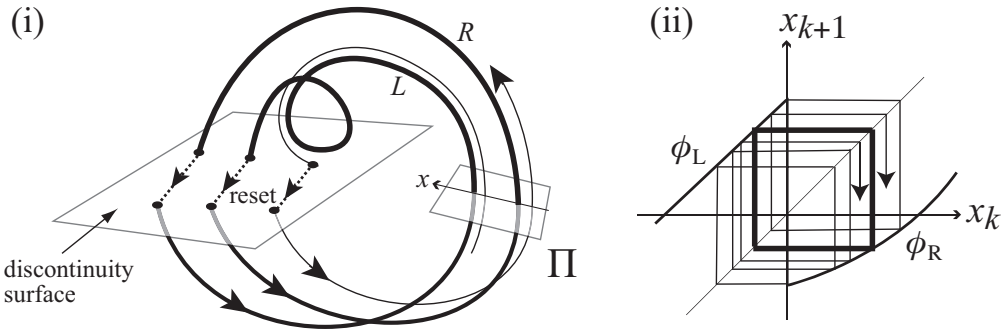

Figure 1: Orbits of period two (bold lines) and period infinity (thin lines) in: (i) a flow with a reset, where only a small piece of the infinite period orbit is shown, and (ii) a one-dimensional map representative of the global flow's return map to the section Π, where several iterates of the infinite period orbit are shown. The infinite period orbit grazes in (i), and intersects the corresponding discontinuity in (ii); it also tends asymptotically towards the period two orbit.

In section 3 we argue that cascades can be understood by studying one-dimensional piecewise-smooth maps of the form

$$x_{i+1} = \phi(x_i) = \begin{cases} \phi_R(x_i) & \text{if} \quad x_i \geq 0, \\ \phi_L(x_i) & \text{if} \quad x_i \leq 0, \end{cases} \tag{1}$$

of the state $x_i \in \mathbb{R}$, over integers i. This is described as a "map with a gap" when $\phi_L(0) \neq \phi_R(0)$ and ϕ_L, ϕ_R, are smooth, with the most interesting dynamics arising when $\phi_L(0) > \phi_R(0)$ (as remarked in [**?**]), that is, when the jump from the left to right branches of the map is negative. We will consider first the case when $\phi_{L,R}$ are linear, and then study the effect of adding nonlinear terms. An orbit is a sequence of iterates $x_0, x_1, ...$ for which $x_{i+1} = \phi(x_i)$. If an orbit makes m visits to $x < 0$, then n visits to $x > 0$, then o visits to $x < 0$, etc., it is given by

$$x_j = ... \circ \phi_L^o \circ \phi_R^n \circ \phi_L^m(x_0),$$

where $j = m + n + o + ...$, and we call x_0 the initial point. It is useful to denote this orbit by a letter sequence $L^m R^n L^o ...$ (reading left to right). An orbit is said to have period p if it satisfies $x_{i+p} = \phi^p(x_i)$.

Given the map (1), it is a simple matter to give conditions for the existence and stability of period one orbits (fixed points, denoted L or R) or period two orbits (denoted L^2, R^2, or LR). In

a piecewise linear map, when ϕ_L and ϕ_R are linear functions of x, a period two orbit must take the form LR (i.e. must cross the discontinuity), and we review the pertinent results in section 4. Orbits of higher period are rather more difficult to describe in general as they may take many different forms. For orbits of the form L^nR or LR^n, regions of existence and stability are known [**?**, **?**]. More generally, if periodic orbits of the form $L^{k-n}R^n$ for $k > n/ \geq 1$ exist, they are known to be unstable for $n > 1$ provided that either: $\phi_L(0) = \phi_R(0)$, in which case (1) is continuous [**?**], or $\phi_L(0) < \phi_R(0)$ [**?**]. Much less is known about the case when $\phi_L(0) > \phi_R(0)$. If $\phi_L(0) > \phi_R(0) > 0$, a class of maps have been shown to undergo period adding cascades to chaos, and formulae for the periods are known [**?**]. If $\phi_L(0) > \phi_R(0) > 0$, then for piecewise linear maps only, an exhaustive study has been made [**?**] that discusses whether finite, infinite, or chaotic attractors exist in different parameter regimes. Detailed results are known only for orbits of the form L^nR or LR^n [**?**, **?**, **?**], which have been shown to exhibit period adding sequences, punctuated by Farey sequences, that lead to chaos. Our study can be considered an extension of these results to periodic orbits of the form $(RL)^nR$ or $(LR)^nL$, and introducing nonlinearity to the map.

The case $\phi_L(0) > \phi_R(0)$ is of sole interest here, for the following reason. We are interested in the maps formed in the presence of grazing, as in figure 9. The map $\phi(x)$ can be thought of as representing the time taken by an orbit to return to a surface containing the point x. An orbit may encounter a discontinuity directly (forming a short orbit, labelled R), or loop around before meeting the discontinuity (a long orbit, labeled L). The two types of orbit, R and L, are separated by a discontinuity in the map associated with grazing. Without loss of generality, one may orient x such that $x > 0$ maps through a short (R) cycle, and $x < 0$ maps through a long (L) cycle. One then expects the presence of a loop to introduce a delay in the flow time relative to grazing, and the absence of a loop to introduce an shortening in the flow time relative to grazing, therefore $\phi_L(0) > 0 > \phi_R(0)$.

Arrangement of the paper:

section 2 cell model

section 3 abstract model, and reduction to 1D

section 4 piecewise linear map: 4.1 invariant interval, 4.2 solutions, 4.3 period 2^n, 4.4 cascade orbits, 4.5 border collision, 4.6 Fareys.

section 5 nonlinear map: 5.1 period 2, 5.2 cascade orbits, 5.3 border collision.

section 6 concluding gubbins.

2 Cascades in models of budding cell cycles

In this section we study cascading behaviour observed in simulations of the following set of ordinary differential equations,

$$\left\{\begin{array}{lcllcl} \dot{u}_1 &=& k_1 - (k_2' + k_2''u_2 + k_2'''u_4)u_1, & \dot{u}_5 &=& k_9 m u_b(1-u_5) - k_{10}u_5, \\ \dot{u}_2 &=& \frac{(k_3'+k_3''u_4)(1-u_2)}{J_3+1-u_2} - \frac{(k_4 m u_b + k_4' u_7)u_2}{J_4+u_2}, & \dot{u}_6 &=& k_{11} - (k_{12}' + k_{12}''u_7 + k_{12}'''m u_b)u_6, \\ \dot{u}_3 &=& k_5' + k_5''\frac{(u_b m)^n}{J_5^n+(u_b m)^n} - k_6 u_3, & \dot{u}_7 &=& k_{13}' + k_{13}''u_8 - k_{14}u_7, \\ \dot{u}_4 &=& \frac{k_7 u_5(u_3-u_4)}{J_7+u_3-u_4} - \frac{k_8 M u_4}{J_8+u_4} - k_6 u_4, & \dot{u}_8 &=& \frac{(k_{15}'m+k_{15}''u_7)(1-u_8)}{J_{15}+1-u_8} - \frac{(k_{16}'+k_{16}''m u_b)u_8}{J_{16}+u_8}, \\ \dot{m} &=& rm\left(1-\frac{m}{\bar{m}}\right), & & & \end{array}\right. \tag{2}$$

where

$$u_b = u_1 - \frac{2u_1u_6}{\Sigma + \sqrt{\Sigma^2 - 4u_1u_6}}, \qquad \Sigma = u_1 + u_6 + \frac{1}{K_{eq}}. \tag{3}$$

The nine quantities u_i and m are scalar variables, and all other quantities are parameters. The system also undergoes a finite state reset

$$g(m) = m/2, \tag{4}$$

applied at the surface

$$h(u) = u_1 - \bar{u}_1, \quad \text{if} \quad \dot{h}(u) = \dot{u}_1 < 0. \tag{5}$$

If an orbit of (2) contains a point at which

$$h(u_1) = 0 \quad \text{and} \quad \dot{h}(u) = \dot{u}_1 = 0, \tag{6}$$

then the orbit is said to *graze* the discontinuity surface $h = 0$.

This model is presented in [**?**] as a serious model of growth and mitosis cycles in cell of budding yeast. The variable m represents the mass of the cell, and the reset event (3) represents cell division. The variables u_i represent concentrations of eight different proteins that activate or inhibit different processes in the cell's cycle of growth. Cell division is triggered when the concentration of cyclin B, $u_1 = [\text{CycB}]_\text{T}$, falls below a critical value $\bar{u}_1$. The remaining concentrations are, symbolically, $u_2 = [\text{Cdh1}]$, $u_3 = [\text{Cdc20}]_\text{T}$, $u_4 = [\text{Cdc20}]_\text{A}$, $u_5 = [\text{IEP}]$, $u_6 = [\text{CKI}]_\text{T}$, $u_7 = [\text{SK}]$, $u_8 = [\text{TF}]$, $u_b = [\text{CycB}]$, $M = [\text{Mad}]$.

There are 39 different parameters in (2)-(3), including rate constants k_i, Michaelis constants J_i, the division threshold $\bar{u}_1$, a growth rate r, and a growth limit $\bar{m}$. The majority of these will be fixed to values considered physically reasonable, given in [**?**] as: $k_1 = 0.04$, $k_2'' = 1$, $k_2''' = 1$, $k_3' = 1$, $k_3'' = 10$, $k_4 = 35$, $k_4' = 2$, $k_5' = 0.005$, $k_5'' = 0.2$, $k_6 = 0.1$, $k_7 = 1$, $k_8 = 0.5$, $k_9 = 0.1$, $k_{10} = 0.02$, $k_{11} = 1$, $k_{12}' = 0.2$, $k_{12}'' = 50$, $k_{12}''' = 100$, $k_{13}' = 0$, $k_{13}'' = 1$, $k_{14} = 1$, $k_{15}' = 1.5$, $k_{15}'' = 0.05$, $k_{16}' = 1$, $k_{16}'' = 3$, $J_3 = 0.04$, $J_4 = 0.04$, $J_5 = 0.3$, $J_7 = 10^{-3}$, $J_8 = 10^{-3}$, $J_{15} = 0.01$, $J_{16} = 0.01$, $K_{eq} = 10^3$, $M = 1$, $\bar{m} = 10$, $r = 0.0165$, $\bar{u} = 0.1$, $n = 4$. We will allow k_2' to vary, observing phenomena over a range from 0.04, the value given in [**?**], to around 0.12. We also take a value of r that differs slightly from the values 0.01 and 0.005 that appear in [**?**].

The phenomenon to be presented will also be demonstrated in a considerable simplification of (2), a four dimensional system

$$\left\{ \begin{array}{rcl} \dot{u}_1 &=& k_1 - k_2' u_1 - k_2'' u_1 u_2, \\ \dot{u}_2 &=& \frac{(k_3' + k_3'' u_3)(1-u_2)}{J_3 + 1 - u_2} - \frac{k_4 u_1 u_2 m}{J_4 + u_2}, \\ \dot{u}_3 &=& k_5' + k_5'' \frac{(u_1 m)^n}{J_5^n + (u_1 m)^n} - k_6 u_3, \\ \dot{m} &=& rm\left(1 - \frac{m}{\bar{m}}\right), \end{array} \right. \tag{7}$$

which is also given in [**?**], and undergoes the same cell division event (3). In simulating this system the parameters will take the same values as given for the full model above, except that we let $r = 0.01$, and will have to consider a wider range of k_2' to observe cascades.

Figure 2 shows a graph of the nine different variables throughout a period two cycle in the system (2). The pattern repeats after the 100 minutes shown, during which the exponentially increasing mass suffers two discontinuities at approximately 55 and 90 minutes, representing cell division. Note the large difference in duration of the long growth period (65 minutes approximately) and the short growth period (35 minutes approximately). Previous studies of the model (see e.g. [**?**, **?**]) typically present only cycles that repeat after a single cell division (period one cycles), or present so-called mutants in which periodic behaviour is typically destroyed by drastically altering the model. In the following, the model will undergo drastic changes of behaviour in the form of

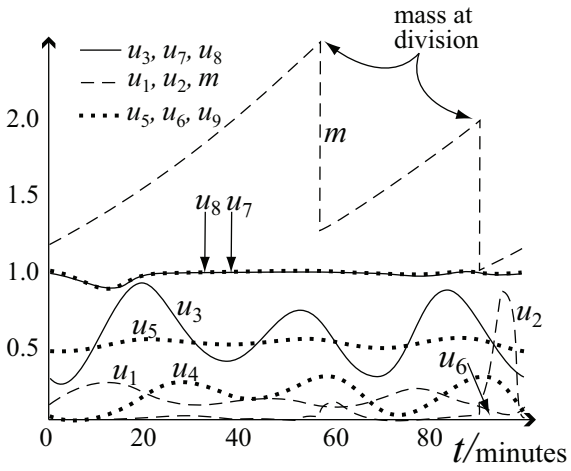

Figure 2: Simulation of the cell cycle (2), showing the (dimensionless) mass m and concentrations u_i, plotted against time in minutes. .

bifurcation cascades, caused, however, by changing a single parameter k_2', smoothly and over a small range.

Figure 3 is a bifurcation diagram that shows periodic orbits of (2)-(3), obtained by the method of shooting, for different values of k_2'. Each point along the diagram represents a periodic orbit passing through the section $h(u) = 0$ in the direction $\dot{h}(u) > 0$, therefore a period p orbit pierces the section p times for a given k_2', and forms p branches in the diagram. The period two orbit graphed in figure 2 forms the pair of branches shown for $k_2' \gtrsim 0.116$. To the left of this, a period adding cascade is observed from left to right, beginning at period one and increasing in multiples of two. This cascade appears to accumulate towards a high period at around $k_2' \approx 0.116$, at which the cascade terminates. Orbits up to period $p = 11$ are clearly identifiable, and raw numerical data (not given) reveals periods of up to 33 within the simulation accuracy.

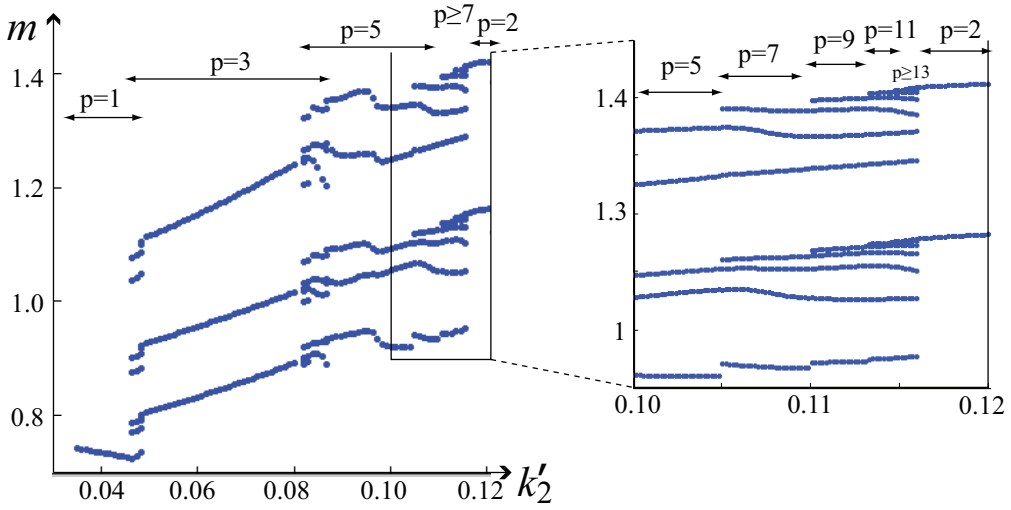

Figure 3: Bifurcation diagram for the simulated system (2). For stable periodic orbits, the value of m is plotted when it crosses the surface $h(u) = 0$ with $\dot{(h)} > 0$, at varying values of k_2'.

Where the ranges of existence of two different periods overlap, one observes orbits whose periods

are sums of multiples of the two periods, known as Farey sequences (see section 4.6). The are clearly seen in figure 3 around $k_2' \approx 0.047$ between the period 1 and 3 orbits, and around $l_2' \approx 0.085$ between period 3 and 5 orbits.

Figure 4 shows simulations of four different orbits in the cascade, in the space of u_1, u_3. For the lower period orbits, the oscillation between long period (with loop, L) cycles and short period (no loop, R) cycles is particularly clear.

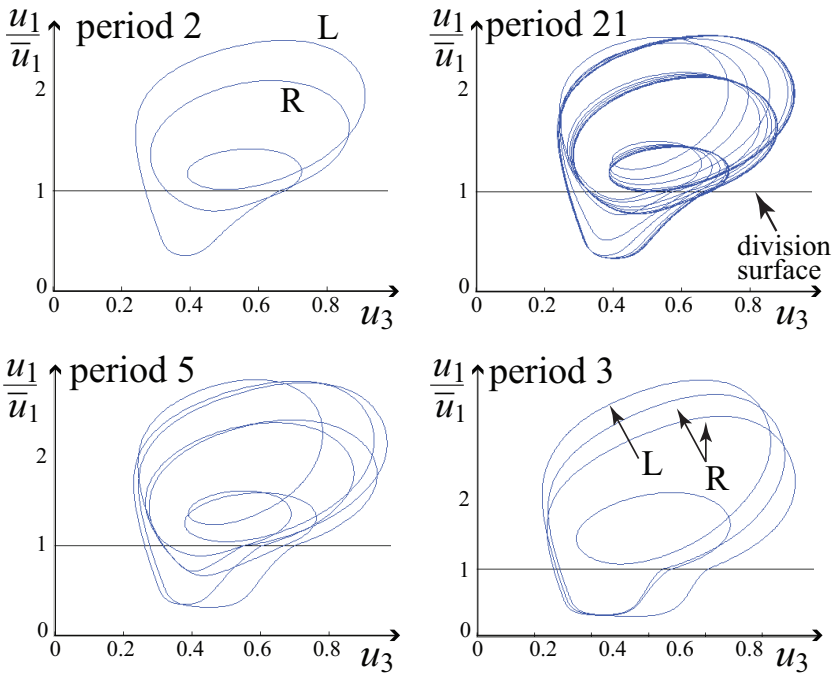

Figure 4: Simulations sampling four different k_2' values from figure 3, showing : (i) a period 2 orbit at $k_2' = 0.118$, (ii) a period 21 orbit at $k_2' = 0.116$, (iii) a period 5 orbit at $k_2' = 0.09$, (iv) a period 3 orbit at $k_2' = 0.07$. The labels L and R indicate periods with and without loops above the division surface respectively.

For the orbits in figure 4, the cobweb diagrams (lines) in figure 5 illustrate successive values of m when the orbit crosses the section $h(u) = 0$, with $\dot{h}(u) > 0$. These are superimposed on an approximation of the return map of m to the same section, obtained by varying m away from the periodic orbit while keeping the starting values of the u_i's fixed, and plotting the value of m (dots) when an orbit returns to the section. The map of m given by the cobweb diagram is seen to follow closely the one-dimensional map thus obtained.

Returning to the bifurcation diagram in figure 3, one can estimate the range of k_2' values for which an orbit of period p exists. The upper bound on k_2' for a period p orbit is given by the righthand extent of a region with p branches in figure 3, and these are listed in Table 1 for $p \geq 15$ (these values are obtained from the raw numerical data that was used to plot figure 3, rather than from visual inspection of the figure). A plot of these values in figure 6 (given over the larger range $p \geq 7$) shows them limiting towards a value of around $k_2' \approx 0.116$.

In section 4.4 it will be shown that the range of existence of an orbit of a given period is governed (in an approximation to be described) by a characteristic scaling. This follows from the existence a quantity

$$v \approx \left(\frac{\mu_\infty - \mu_b}{\mu_\infty - \mu_a} \right)^{\frac{2}{b-a}} , \tag{8}$$

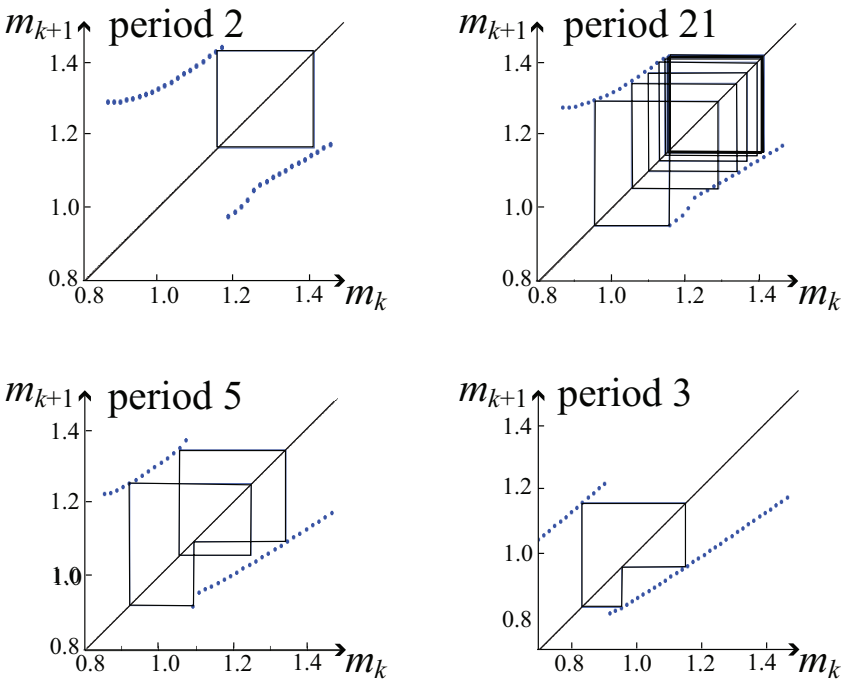

Figure 5: Maps of the mass, plotting return values against initial values of m, on the surface $h(u) = 0$ with $\dot{h}(u) > 0$. The four simulations correspond to those in figure 4. The cobweb lines join successive values of m in a periodic orbit, and the dots are return values of m obtained by shooting.

p	15	17	19	21	23	25	27	33
k_2'	0.1154	0.11577	0.11590	0.11600	0.116034	0.116048	0.116054	0.116058

Table 1: List of k_2' values at the righthand end of the branch of period p, from a simulation of (2) (parameter values given in the text). The estimation error is ± 1 on the last decimal place. The periods 29 and 31 are missing, having not been detected in the simulation.

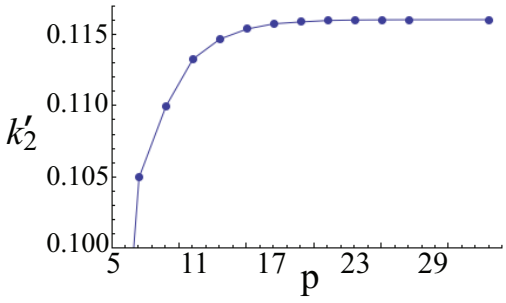

Figure 6: A plot of Table 1, showing k_2' parameter values at which each branch vanishes in figure 3, plotted against the relevent period.

that relates the upper bounds, μ_a and μ_b, of some parameter, μ, measured relative to some μ_∞, for which orbits of period a and b exist. The quantity v is independent of the periods a and b, or any other parameters of the system, so (8) provides a characteristic scaling of the system, in which μ can be directly substituted with whichever parameter we are interested in varying, in this case k_2'. By equating the righthand sides for two different integer pairs (a, b) and (a', b'), one can

eliminate v, and solve numerically to find the value of μ_∞. Moreover, if we choose a, b, a', b' such that $b - a = b' - a' = 2r$ for some integer r, we can solve explicitly to find

$$\mu_\infty = \frac{\mu_{a+2r}\mu_{a'} - \mu_{a'+2r}\mu_a}{\mu_{a+2r} + \mu_{a'} - \mu_{a'+2r} - \mu_a} + \mathsf{O}\left(v^{\frac{a+1}{2}}\right). \tag{9}$$

This simplifies further if we let two of the periods be equal, for example setting $a' = a + 2r$, thus requiring only three different μ values, μ_a, μ_{a+2r}, and μ_{a+4r}, to determine μ_∞ uniquely. Replacing μ with k_2' and using triples of values from Table 1, one obtains several estimates of the value of $k_{2\infty}'$ (given by μ_∞), a sample of which are shown in Table 2. The estimate changes slightly depending on the three periods chosen, because (8) and (9) are only an approximate characterization of the system. This is partly due to possible numerical error in estimating the values in Table 1, but also because the analysis that leads to (9) is accurate only for higher period orbits, and therefore should improve down through the rows in Table 2.

periods	$k_{2\infty}'$
$15, 17, 19$	0.11497 ± 10^{-4}
$17, 19, 21$	0.116333 ± 10^{-5}
$19, 21, 23$	0.116052 ± 10^{-5}
$21, 23, 25$	0.116058 ± 10^{-5}
$23, 25, 27$	0.116059 ± 10^{-6}
$25, 27, 33$	0.116058 ± 10^{-6}

Table 2: Value of k_2' at which the period two orbit grazes, $k_{2\infty}'$, estimated for the three periods listed, using (9) for all but the last row, which uses a numerical solution from (8). Errors follow from Table 1.

The critical k_2' value, $k_{2\infty}'$, is the parameter value at which the allowed period of orbits in the cascade becomes infinite. This causes the accumulation of branches of periodic orbits observed near $k_2' \approx 0.116$ in figure 3, and the estimates in Table 2 refine this value to $k_2' = 0.116058$. The accuracy of these predictions is verified by observing the accumulation of branches that occurs at this value of k_2' in figure 3. The precision of this value could be improved by a finer simulation to find the end points in Table 1 than was used for these calculations.

Figure 7 shows a similar cascade in a simulation of the four dimensional model (7). This bifurcation diagram appears to have more clearly formed branches than the full model, due to its simpler dynamics. A more crucial difference exists here, however, as is seen by close inspection of the period two orbits in each case, which appear for $k_2' \gtrsim 0.116$ in figure 3 and $k_2' \gtrsim 0.15394$ in figure 7. In figure 3, only *two* branches are seen to the right of the cascade, caused by a stable period two orbit, and these branches appear to have a finite gradient everywhere. In figure 7, there are now *four* branches to the right of the cascade, with a vertical gradient where they emerge from the cascade at $k_2' \approx 0.15394$, forming two continuous curves. This indicates a saddle-node bifurcation, and indeed only the upper of each curve represents a stable orbit, the lower branch being an unstable orbit (to obtain this branch, continuation methods were used rather than shooting). A similar analysis of the cascade's scaling can be applied as that performed above; the appropriate formulae will be derived in section 5.2.

In summary, similar cascades are observed in the two different models (2) and (7) together with (3). In one case, periodic orbits of increasing odd period are seen to accumulate at a parameter value $k_2' \approx 0.116058$, at which a stable period two orbit is created. Figure 8 shows that the lefthand extreme of each branch appears at a grazing orbit, that is, when an orbit has a minimum of h at

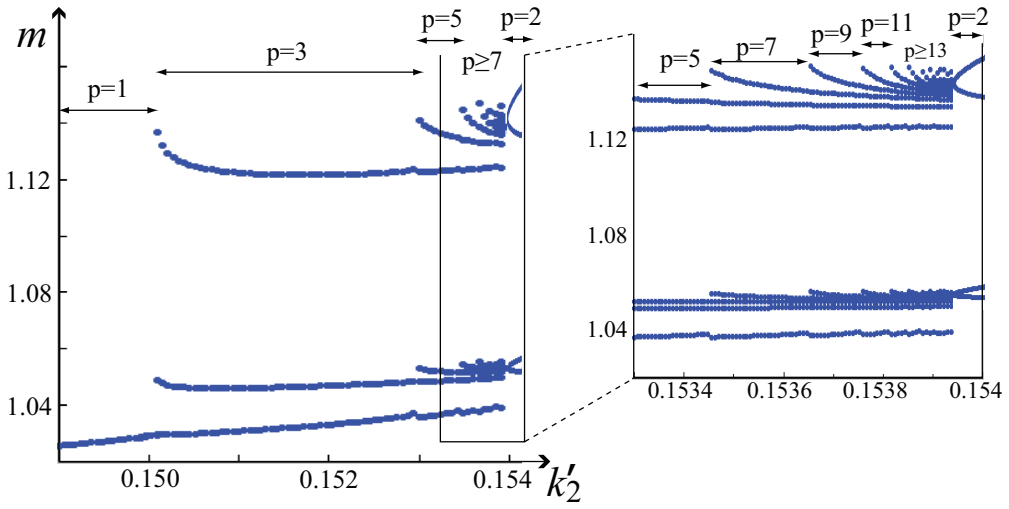

Figure 7: Bifurcation diagram for the simulated system (7). For orbits of period p, the value of m is plotted when it crosses the surface $u_1 = \bar{u}_1$ with $\dot{u}_1 > 0$, at changing values of k_2'. All orbits are stable, except the lower branch of period two orbits, which collide with the stable upper branch in a saddle-node bifurcation at around $k_2' = 0.15387$.

$h(u) = 0$. This applies to the orbits in the cascade (as far as the precision of the simulation can determine) and to the period two orbit. The simpler model again sees accumulation towards a particular value, $k_2' \approx 0.15394$, but in this case a pair of period two orbits are created, the mechanism of their creation is a saddle-node bifurcation, and as figure 8 shows, neither of these are grazing (note that orbits inside the cascade to the left of $k_2' \approx 0.15394$ do still appear from grazing).

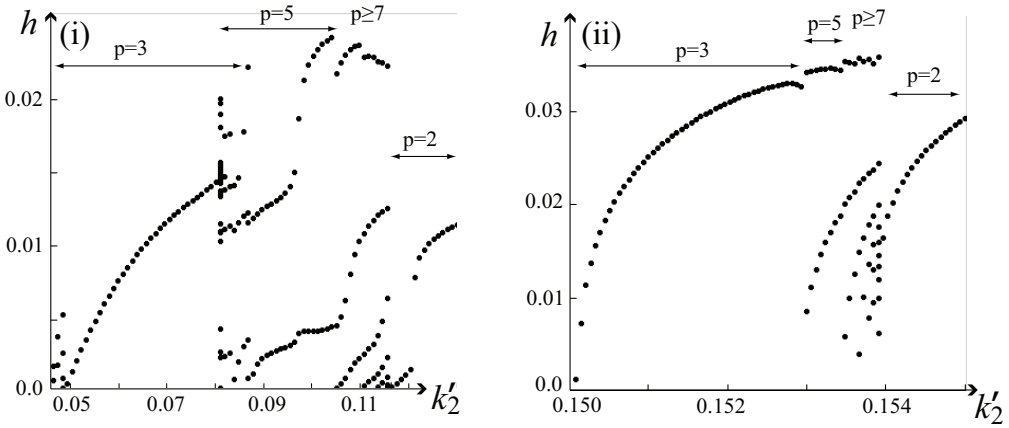

Figure 8: Bifurcation diagrams corresponding to: (i) figure 3, and (ii) figure 7; showing $h(u)$ at minima along the orbits, that is when $\dot{h}(u) = 0 < \ddot{h}(u)$.

These two cascade phenomena appear robust enough to be observed over a range of different values of the 39 parameters in the full model, or the 16 parameters in the simplified model. The phenomenon is also quite robust under alterations in the division rule, (3), to fractions other than 1/2. It is, however, possible for more complex cascades to occur, as we discuss in section 6. In particular, the orbits considered above form only one small loop above $h(u) = 0$ between successive divisions (see figure 4). By increasing r, the strength of rotation in the system is increased, and this causes periodic orbits to loop many times between divisions, increasing the complexity of the

cascade.

To gain insight into the origin of these two bifurcation sequences, and to see where the scaling laws (8) and (9) used above came from, in the next section we discuss an abstract description of the flows above, and argue that the cascade can be understood by simplfying the flow to a one dimensional map with a discontinuity.

3 Reduction to a one-dimensional map

We begin by setting up an abstract form of the system in section 2. Let a scalar variable, x, and an $n-1$ dimensional state variable, y, evolve according to a hybrid dynamical system,

$$\begin{aligned} \dot{x} &= f(x), && (10)\\ \dot{y} &= F(x,y), && (11)\\ x &\mapsto g(x) \quad \text{when} \quad h(y)=0>\dot{h}(y), && (12) \end{aligned}$$

where F is a smooth vector field, while f, g, and h are smooth scalar functions. We assume

$$f > 0 \tag{13}$$

throughout the region of interest. The time derivative $\dot{h}$ is given by the Lie derivative along the flow of F,

$$\dot{h}(y) = \mathcal{L}_F h(y) = F(x,y)\cdot\frac{d}{dy}h(y).$$

Thus the system consists of a set of ordinary equations, (10)-(11), interrupted by a discrete event, (12), called the *reset*. The scalar function h is regular in y, meaning $\frac{dh}{dy}\neq 0$.

Let there exist a state $y=\tilde{y}^*$ to which the flow is strongly attracted, but which, since x varies independently of y, does not form an asymptotic attractor. More precisely, let there exist a locally defined section Π through the flow (see figure 1(i)), coordinatized by the scalar x and an $n-2$ dimensional variable $\tilde{y}$. Let a pair of return maps $(\phi,\Psi):\Pi\mapsto\Pi$ give the point $(\phi(x,\tilde{y}),\Psi(x,\tilde{y}))$ at which the hybrid flow (10)-(12) through a point $(x,\tilde{y})\in\Pi$ returns to Π, where ϕ is a scalar and Ψ is $n-2$ dimensional. Let there exist a set of points $\{(x,\tilde{y}^*)\in\Pi:\ x\in\mathbb{R}\}$ on which the eigenvalues, c_j for $j=1,...,n-2$, of the Jacobian derivative $\frac{d\,\Psi}{d(x,\tilde{y})}$ at $(x,\tilde{y}^*)$, satisfy $|c_j|\ll 1$. Then $\tilde{y}\approx\tilde{y}^*$ after sufficiently many iterations of the maps ϕ and Ψ, so Ψ approaches the identity. The flow is then well approximated by neglecting y, and treating ϕ as a one dimensional map of the variable x.

In the biological models considered in section 2, this situation seems to arise because the $n-1$ variables y, (u in the cell model), are strongly coupled and tend to a fixed value, while one variable x, (m in the cell model), varies independently except at the discontinuity. The only influence of y on x is in determining the time instant at which the discontinuity (cell division) occurs.

We have then to determine the typical from that the map ϕ will take. For this we must examine the dynamics elsewhere than the section Π. Let us label the reset surface

$$\Sigma = \{(x,y)\in\mathbb{R}^n\ :\ h(y)=0\}, \tag{14}$$

and then identify the turning surface

$$\Gamma = \{(x,y)\in\mathbb{R}^n:\ \mathcal{L}_f h(y)=0\}, \tag{15}$$

where orbits of (10) turn around with respect to Σ. Their intersection forms a *grazing set*, $\Gamma\cap\Sigma$, where orbits contact the reset surface with zero normal velocity. The sets Σ and Γ are $n-1$ dimensional hypersurfaces, illustrated for $n=3$ in figure 9.

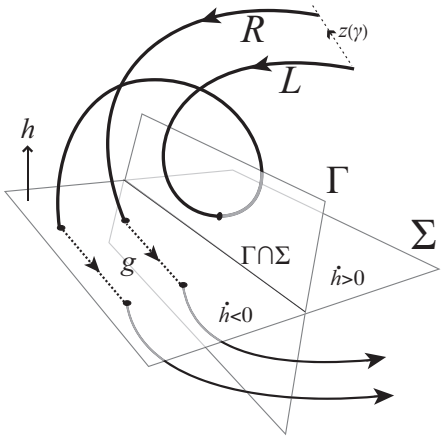

Figure 9: A hybrid system with a switch at Σ. Under a small change in initial condition, the flow may either intersect the reset surface first, or cross a turning surface, Γ, before reaching Σ. This advances/delays the reset, g, as a loop is removed/added between the long-cycle L, and short-cycle R. In a biological cell cycle model [**?**]: g is cell division, while L and R give rise to long and short growth cycles. A path $z(\gamma)$ as discussed in the text is shown.

Consider the orbit from some initial point, $(x, y) = z$, to cross Γ at two points, first where $h(y)\mathcal{L}_F^2 h(y) < 0$ (turning away from Σ) and then where $h(y)\mathcal{L}_F^2 h(y) > 0$ (turning towards Σ), before reaching Σ at time $t = T(z)$. Such an orbit forms a loop on one side of Σ before the reset (12) occurs (the orbit L in figure 9). Now let the initial point z follow a path $z(\gamma)$ such that, as we vary the scalar parameter γ, the first point of intersection with the turning surface Γ can be brought closer to Σ, until the orbit hits Σ before it can cross Γ (orbit R in figure 9). This prevents the orbit forming a loop, and advances the reset time $T(z(\gamma))$ by a discrete amount. This jump in the value of T occurs at a parameter $\gamma = \gamma_g$, for which the orbit through $z(\gamma)$ intersects the grazing set $\Gamma \cap \Sigma$, local to which we can express T as

$$T(\gamma) = \begin{cases} T_R(\gamma), & \text{if} \quad \gamma \geq \gamma_g, \\ T_L(\gamma), & \text{if} \quad \gamma \leq \gamma_g, \end{cases} \tag{16}$$

where T_L and T_R are smooth single-valued functions. Let us now consider the map described above, $\phi(x)$, which describes the return value of x to some section Π through the flow. Since x grows monotonically in time by (13), except for the discontinuity whose affect on the flow time is described by (16), then we obtain a general form for the map ϕ as

$$\phi(\gamma) = \begin{cases} \phi_R(\gamma), & \text{if} \quad \gamma \geq \gamma_g, \\ \phi_L(\gamma), & \text{if} \quad \gamma \leq \gamma_g. \end{cases} \tag{17}$$

Thus the maps ϕ_L and ϕ_R give the points where long (L) and short (R) orbits return to Π. In sections 4 and 5, we show that maps of this form can exhibit bifurcations that account for the cascades observed in the biological model in section 2, approximating them first as piecewise linear near the discontinuity, and then considering the effect of nonlinearity. This can be extended to orbits that intersect Γ many times between resets, forming even longer periods and involving further discontinuities; these are discussed briefly in section 6.

3.1 Geometry of a cascade

Above we have argued that a one dimensional piecewise smooth map can represent certain features of the global dynamics of a class of n-dimensional flows. We have not yet identified the essential

features of the flow, or the map, that gives rise to cascades of the form seen in the cell model. We describe these qualitatively here. In the next section we will prove that such conditions in a one dimensional map are sufficient for cascades.

By a period p orbit, we will mean a solution of the system (10)-(12) that repeats after p intersections with the discontinuity surface $h(u) = 0$.

In a flow parameterized by μ, the key necessary conditions for cascades near some $\mu = \mu_\infty$ appear to be:

(i) there exists an invariant region $\mathcal{I}$ that contains all orbits through some set of grazing points $G \subset \Gamma \cap \Sigma$,

(ii) for $\mu \leq \mu_\infty$, $\mathcal{I}$ also contains a stable orbit whose period is finite,

(iii) for $\mu \geq \mu_\infty$, the set G is an attractor of the return map of the flow to the hypersurface Γ.

When the finite period orbit vanishes for $\mu > \mu_\infty$, the invariance of $\mathcal{I}$ causes a new global attractor to be created. The vanished periodic orbit leaves behind the mirage of an attractor on the set G: orbits are attracted towards G each time they intersect Γ as if G is an attractor, but ultimately overshoot and hit Σ, at which they undergo a reset event, and yet remain confined to $\mathcal{I}$.

In the scenarios considered in section 2, 4, and 5, the stable orbit in (i) has period two, and vanishes at $\mu = \mu_\infty$ either by grazing, in which case it instersects the set G, or by saddle-node bifurcation, in which case the centre manifold of the bifurcation intersects G. The attractivity of G at $\mu = \mu_\infty$ creates an additional stable orbit that has a point in G, and asymptotes towards the period two orbit, intersecting Γ and Σ infinitely many times to form an infinite period grazing orbit. For $\mu > \mu_\infty$ this periodic orbit undergoes a bifurcation cascade in which its period becomes finite, and decreases through odd integers as $\mu - \mu_\infty$ increases; these period adding bifurcations occur each time the orbit intersects G.

In figure 10, we illustrate this geometry in a higher dimensional flow representative of the cell model, and also in a one-dimensional map, which we study in detail in sections 4-5. The figure illustrates dynamics around a grazing set G, on an invariant set $\mathcal{I}$ (in figure 10(ii), $\mathcal{I}$ consists of all orbits through the shaded regions) . An open set $P \subset \Sigma$ maps to an open set $P_\Gamma \cup P_\Sigma$ under the flow, where $P_\Gamma \subset \Gamma$ and $P_\Sigma \subset \Sigma$, and such that the set of grazing points $G = P_\Sigma \cap P_\Gamma$ maps into the interior of P under the reset map on Σ. Then the generator of the invariant set $\mathcal{I}$ can be taken as the set of points $x \in P_\Sigma \cup P_\Gamma$ in the neighbourhood of G that map into the interior of P.

In figure 11, we illustrate two scenarios by which such mirages of attractors form when a period two orbit is destroyed either by grazing, or by a saddle-node bifurcation. In the gazing case, a periodic orbit through the points p_1 and p_1' undergoes grazing when p_1 enters the set G, after which G attracts orbits that intersect Γ on a set $P \subset \Gamma$. Orbits attracted towards G overshoot, undergo the reset into the neighbourhood of a set $H' \subset P'$, which maps under the flow back into P. In the saddle-node case, stable and unstable periodic orbits through the points p_1, p_1', and p_2, p_2', respectively, collide in a saddle-node bifurcation, the centre manifold of which intersects the set G. Afterwards, G attracts orbits that intersect Γ on a set $P \subset \Gamma$, similarly to the grazing case. In both cases, the result of G being attractive, but not asymptotically so, allowing orbits to overshoot G, seems to create high periodic orbits. In simple cases, namely those in section 3 above and in the maps of sections 4-5, the result is a cascade of orbits of decreasing period. We now turn to a detailed study of these maps as sources of cascades.

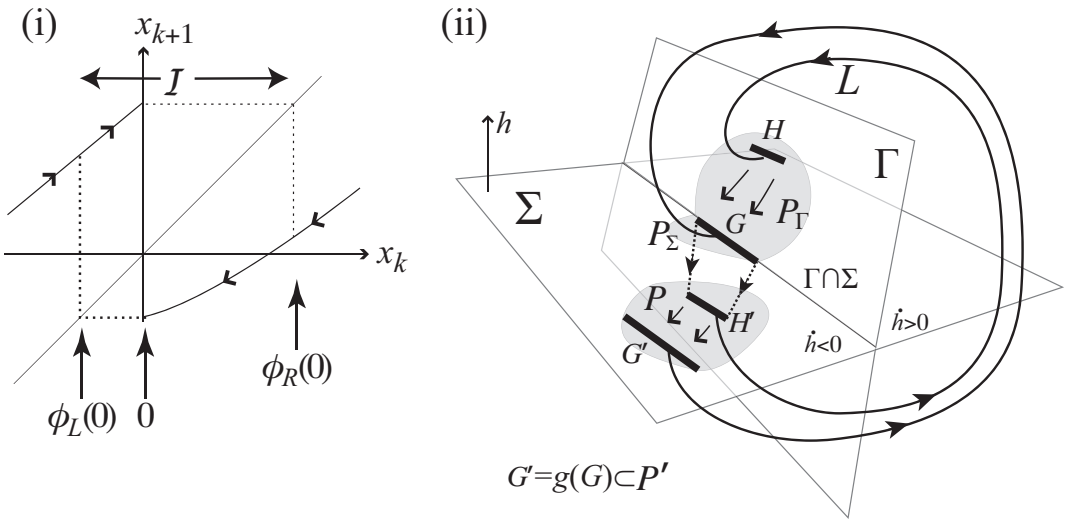

Figure 10: The mirage of an attractor at the grazing boundary. The conditions for a cascade are illustrated: after a period two orbit vanishes, its domain of attraction leaves behind sets, P_Σ and P_Γ, attracted towards the a grazing set $G \subset \Gamma \cap \Sigma$; points in P_Σ in the neighbourhood of G, which have reset values in a neighbourhood of $H' = g(G)$, must return to P_Γ under the flow.

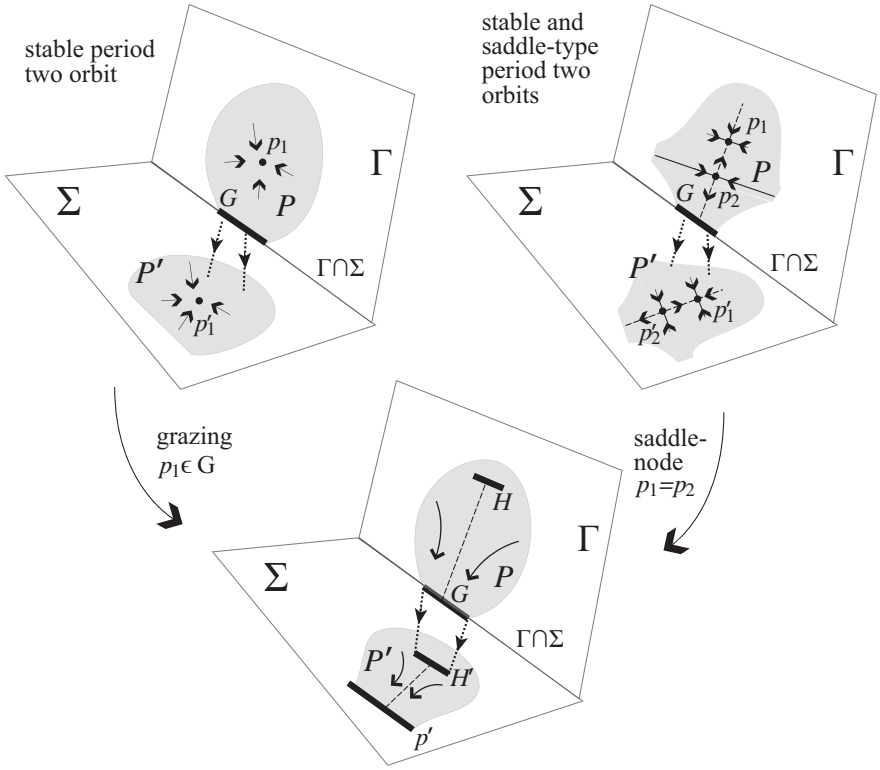

Figure 11: p_1 and p_1' are points along a stable period two orbit, with domains of attraction P_1 and P_1'. As a parameter changes the period two orbit is destroyed, either by grazing (left) or by a saddle-node bifurcation (right). Grazing automatically creates an attractive set of grazing points, G. The saddle-node creates an attractive set of grazing points, G, if the saddle's unstable manifold, lying in the centre manifold of the bifurcation (dashed), transversally intersects the grazing set $\Gamma \cap \Sigma$.

4 Piecewise linear map with a gap

We begin by studying the piecewise linear map

$$x_{i+1} = \begin{cases} \phi_R(x_i) = \mu + \lambda + v_R x_i & \text{if} \quad x_i \geq 0, \\ \phi_L(x_i) = \mu + v_L x_i & \text{if} \quad x_i \leq 0. \end{cases} \tag{18}$$

where we assume $\phi_L(0) > \phi_R(0)$, in which case x can be scaled such that the jump in the map at $x = 0$ is $\lambda = -1$, though we leave the symbol λ in for convenience.

Unlike many previous studies, we allow both ϕ_R and ϕ_L to be applied at the discontinuity. Although this means the solution of the map is non-unique at $x = 0$, it is useful to consider the two solutions as giving the limiting behaviour of the map as x tends to 0 from above and from below, since arbitrarily close to the limit, the solutions on both sides are well defined.

It will be shown that there exists a parameter $\mu = \mu_\infty$ at which the map satisfies:

$$\text{(i)} \qquad \phi_R \circ \phi_L(0) = 0, \text{ and} \tag{19}$$

$$\text{(iii)} \qquad \phi_R \circ (\phi_L \circ \phi_R)^n(0) \to 0 \quad \text{as} \quad n \to 0. \tag{20}$$

Condition (i) defines a period two orbit, and (ii) can be described as an orbit of infinite period. Both orbits have an iterate on the discontinuity, so that a border collision occurs at $\mu = \mu_\infty$.

The analysis in this section can be considered as an extension of previous studies, which analysed periodic orbits of the form $R^n L$ given by $\phi_R^n \circ \phi_L(x) = x$ (or similarly $L^n R$), whereas here we study periodic orbits of the form $(RL)^n$, given by $(\phi_R \circ \phi_L)^n(x) = x$, and of the form $(RL)^n R$, given by $\phi_R \circ (\phi_R \circ \phi_L)^n(x) = x$. All of the following analysis can be extended to orbits of the form $(LR)^n$ and $(LR)^n L$ by making the substitution $\{x, v_R, v_L, \mu\} \mapsto \{-x, v_L, v_R, -\mu - \lambda\}$.

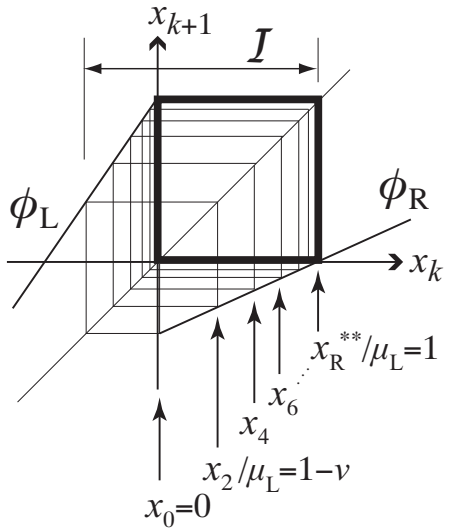

Figure 12: The period two orbit (bold lines) defined in (19), and the infinite period orbit (fine lines) defined in (20), both diverging from each other and recombining at the discontinuity, $x = 0$. The quantities v, μ_L, x_R^{**}, are defined in section 4.3.

4.1 Invariance of the interval $[\phi_R(0),\ \phi_L(0)]$

Conditions (20) requires that an application of ϕ_R at the point $x = 0$ is followed by ϕ_L, which only occurs if $\phi_R(0) < 0 < \phi_L(0)$. From (18) we have $\phi_R(0) = \mu + \lambda$, and therefore $\mu + \lambda < 0 < \mu$, or

simply

$$0 < \mu < -\lambda. \tag{21}$$

Moreover, given $\phi_R \circ \phi_L(0) = 0$ by (19), the existence of a solution (20) requires $(\phi_L \circ \phi_R(0))^n > 0$ for all $k = 1, ..., n$. Taking $n = 1$ gives the condition

$$\phi_L \circ \phi_R(0) = \mu + v_L(\mu + \lambda) < 0,$$

and substituting the value of μ for which $\phi_R \circ \phi_L(0) = 0$ by (19), which is easily found to be $\mu = -\lambda/(1 + v_R)$, yields the condition

$$|v| < 1. \tag{22}$$

This is therefore required for the existence of the infinite period orbit (20) with an iterate on the discontinuity. In the next section we will see that then $(\phi_L \circ \phi_R(0))^n > 0$ for each power n, provided that the interval

$$\mathcal{I} \;=\; [\phi_R(0),\; \phi_L(0)] \;=\; [\mu + \lambda,\; \mu] \tag{23}$$

is invariant under the map (18). Invariance of $\mathcal{I}$ requires that the values of the gradients $v_{R,L}$ are restricted to

$$0 < v_R < -\frac{\lambda}{\mu}, \qquad 0 < v_L < -\frac{\lambda}{\mu + \lambda}. \tag{24}$$

To prove this, we first show that each of the functions $\phi_{R,L}$ map points $x \in \mathcal{I}$ towards $x = 0$, that is, we show that $\phi_R(x) - x < 0$ and $\phi_L(x) - x > 0$ for $x \in \mathcal{I}$. For the former we have

$$\begin{aligned}
\phi_R(x) - x &= \mu + \lambda + (v_R - 1)x && \text{by (18)} \\
&< \mu + \lambda - \left(\frac{\lambda}{\mu} + 1\right) x && \text{by (24)} \\
&= (\mu + \lambda)\left(1 - \frac{x}{\mu}\right) \\
&< 0 && \text{by (21) and } x \in \mathcal{I}.
\end{aligned} \tag{25}$$

In the last line, we use from (21) that $\mu + \lambda < 0$ and $\mu > 0$, while $x \in \mathcal{I}$ implies $\frac{x}{\mu} < 1$. For the L map we have

$$\begin{aligned}
\phi_L(x) - x &= \mu + (v_L - 1)x && \text{by (18)} \\
&> \mu - x && \text{by (24)} \\
&> 0 && \text{by (21) and } x < 0.
\end{aligned} \tag{26}$$

Having been mapped towards $x = 0$, any point must again map to the interior of $\mathcal{I}$, since $\phi_{L,R}(0) \in \mathcal{I}$ by definition (23). Therefore under the conditions (21) and (22), the interval $\mathcal{I} = [\phi_R(0), \phi_L(0)]$ is invariant.

Fixed points of the map (18) lie at $x = x_R^* := \frac{\mu+\lambda}{1-v_R}$ and $x = x_L^* := \frac{\mu}{1-v_L}$, exist if and only if $x_L^* < 0 < x_R^*$, and are stable if $|v_{R,L}| < 1$. It follows from (24) that no fixed points $x_{R,L}^*$ can exist within the invariant interval $\mathcal{I}$, and we will not study these further.

4.2 Solutions of the piecewise linear map

If an orbit of (18) does not cross $x = 0$ from an initial point x_0 until the r^{th} iterate x_r, then x_r is given by

$$x_r(\mu, x_0) = \begin{cases} (\phi_R)^r(x_0) = v_R^r x_0 + \frac{1-v_R^r}{1-v_R}(\mu + \lambda) & \text{if } x_0 \geq 0, \\ (\phi_L)^r(x_0) = v_L^r x_0 + \frac{1-v_L^r}{1-v_L}\mu & \text{if } x_0 \leq 0, \end{cases} \tag{27}$$

where $r \geq 1$ is an integer. Since this is only valid if all iterates x_i have the same sign for $i = 0, ..., r-1$, the domain of $x_r(\mu, x_0)$ is given by the regions $x_0 > \frac{(\mu+\lambda)(1-v_R^{-r})}{1-v_R}$ and $x_0 < \frac{\mu(1-v_L^{-r})}{1-v_L}$. The proof of this is simple given that these maps are linear in x_0; the details are omitted as this result will not be used here.

If, instead, an orbit starting at x_0 crosses $x = 0$, we can define a second iterate map given by

$$x_{i+2} = \begin{cases} \Phi_R(x_i) = \phi_L \circ \phi_R(x_i) & \text{if} \quad x_i \geq 0, \\ \Phi_L(x_i) = \phi_R \circ \phi_L(x_i) & \text{if} \quad x_i \leq 0. \end{cases} \tag{28}$$

Solving (28) by substituting in (18), after $2n$ iterations we find the orbit of an initial point x_0 to be given by

$$x_{2n}(\mu, x_0) = \begin{cases} (\Phi_R)^n(x_0) = v^n x_0 + \frac{1-v^n}{1-v}\left(1 - \frac{\mu}{\mu_R}\right)\lambda v_L & \text{if} \quad x_0 \geq 0, \\ (\Phi_L)^n(x_0) = v^n x_0 + \frac{1-v^n}{1-v}\left(1 - \frac{\mu}{\mu_L}\right)\lambda & \text{if} \quad x_0 \leq 0, \end{cases} \tag{29}$$

where $n \geq 1$ is an integer, and we introduce three parameters

$$\mu_L = -\frac{\lambda}{1+v_R}, \qquad \mu_R = -\frac{\lambda v_L}{1+v_L}, \qquad \text{and} \qquad v = v_R v_L. \tag{30}$$

For reasons that will become clear, we will frequently give expressions in terms of the parameters $\mu_{R,L}$ and v, in place of $v_{R,L}$.

The condition for the existence of solutions of the form (29) is that there is a sign change between each x_i and $x_{i+1} = \phi_{L,R}(x_i)$, that is, $x_{2n} = \Phi_{L,R}(x_0)$ exists if and only if

$$x_i \, \phi_{R,L}(x_i) < 0, \quad \text{for all} \;\; i = 0, 2, 4, ..., n-2. \tag{31}$$

By combining the formulae (27) and (29), orbits with an arbitrary form can be described, but we will not make use of (27) here.

4.3 Orbits of period two

In this section we consider periodic orbits of the form $(RL)^n$ for a general integer n, and derive an expression for stable period two orbits which, at a certain parameter, undergo a border collision satisfying condition (19).

Periodic orbits of the form $(RL)^n$ are fixed points of the map (29), given by

$$x_L^{**} = \frac{\xi(\mu) - \mu}{v_L} = \frac{\lambda}{1-v}\left(1 - \frac{\mu}{\mu_L}\right), \quad x_R^{**} = \xi(\mu) := \frac{\lambda v_L}{1-v}\left(1 - \frac{\mu}{\mu_R}\right), \tag{32}$$

where we define the function $\xi(\mu)$. Since these iterates are independent of n, they represent only two fixed points, one either side of $x = 0$, hence these orbits have period two. They exist if and only if

$$(\xi(\mu) - \mu)/v_L < 0 < \xi(\mu), \tag{33}$$

and are stable because the derivative of the second iterate map, $\frac{d\Phi_{L,R}}{dx_0} = v$, has modulus less than unity by (22). From (22) and (24) it is clear that $\frac{\lambda}{1-v}$ and $\frac{\lambda v_L}{1-v}$ are positive quantities, therefore substituting (32) into (33) and simplifying, the existence condition for stable period two orbits becomes

$$\mu_R \leq \mu \leq \mu_L. \tag{34}$$

Such a range of μ is possible, since substituting (30) into (22) shows that the parameters $\mu_{R,L}$ are strictly ordered according to

$$\mu_R < \mu_L. \tag{35}$$

Again taking (32), applying (34) and (22), a little algebra gives

$$\mu + \lambda \leq x_L^{**} \leq 0 \leq x_R^{**} \leq \mu, \tag{36}$$

meaning that the period two orbit, (x_L^{**}, x_R^{**}), lies inside the invariant interval $\mathcal{I} = [\mu + \lambda, \mu]$.

To summarize, while μ lies inside the bounds (34), a period two orbit exists, by (22) it is stable, and the map has a well defined local derivative in the neighbourhood of $x_{R,L}^{**}$. We also have from (29) that, from any initial point x_0, the second iterate map obeys

$$x_{2n} \to x_{R,L}^{**} \qquad \text{as} \quad n \to \infty. \tag{37}$$

Thus the domain of attraction of the period two orbit is the entire domain of $\Phi^{\pm}$, which, however, is not easy to express explicitly. If there exist no other attractors inside the interval $\mathcal{I}$, then the perioid two orbit's period domain of attraction includes the whole interval $\mathcal{I}$. This is as observed in simulation, however a definitive proof must exclude the possibility of periodic orbits of any form from $\mathcal{I}$ (the conditions (24) at least exclude fixed points); such a result is not pursued here and we assume no other attractors exist for $\mu_R < \mu < \mu_L$.

A border collision occurs when $\mu = \mu_R$ or μ_L, as we discuss in section 4.5.

4.4 Orbits of the form $(RL)^n R$

In this section we consider periodic orbits with the form $(RL)^n R$, for a general integer n.

For a solution of (18) with the form $(RL)^n R$, the $(2n+1)^{th}$ iterate is given by

$$x_{2n+1}(\mu, x_0) = \phi_R \circ (\phi_L \circ \phi_R)^n = \mu + \lambda + v_R x_{2n}(\mu, x_0), \tag{38}$$

that is, n applications of the second iterate map $\Phi_R = \phi_L \circ \phi_R$ from (29), followed by a single application of ϕ_R. Expanding this by substituting in (29), some re-arrangement gives

$$x_{2n+1}(\mu, x_0) = v_R v^n x_0 + \frac{\left(1 - \frac{\mu}{\mu_L}\right) - \left(1 - \frac{\mu}{\mu_R}\right) v^{n+1}}{1 - v} \lambda. \tag{39}$$

If they are valid solutions of the map (18), then fixed points of (39) correspond to iterates lying on period $\kappa = 2n + 1$ orbits of (18). We label such a fixed point x_κ, then solve $x_{2n+1}(x_\kappa) = x_\kappa$ to find

$$x_\kappa(\mu) = \frac{\left(1 - \frac{\mu}{\mu_L}\right) - \left(1 - \frac{\mu}{\mu_R}\right) v^{\frac{\kappa+1}{2}}}{(1 - v)(1 - v_R v^{\frac{\kappa+1}{2}})} \lambda. \tag{40}$$

The map, and an orbit of period $\kappa = 5$, are illustrated in figure 13.

Given that the map (39) is linear it has the form $x_\kappa^{\pm} = a x_0 + b$ for constants a and b, and its fixed points are stable if $|a| < 1$. Applying this to (39), where $a = v_R v^{\frac{\kappa+1}{2}}$, and using (24) to place an upper bound on v_R, gives the stability condition

$$v^{\frac{\kappa+1}{2}} < -\mu/\lambda, \tag{41}$$

where the righthand side is strictly positive (since $\lambda < 0$ by definition and $\mu > 0$ by (21)). Thus a period κ orbit, if it exists, is stable if it satisfies (41). Note that periodic orbits with sufficiently

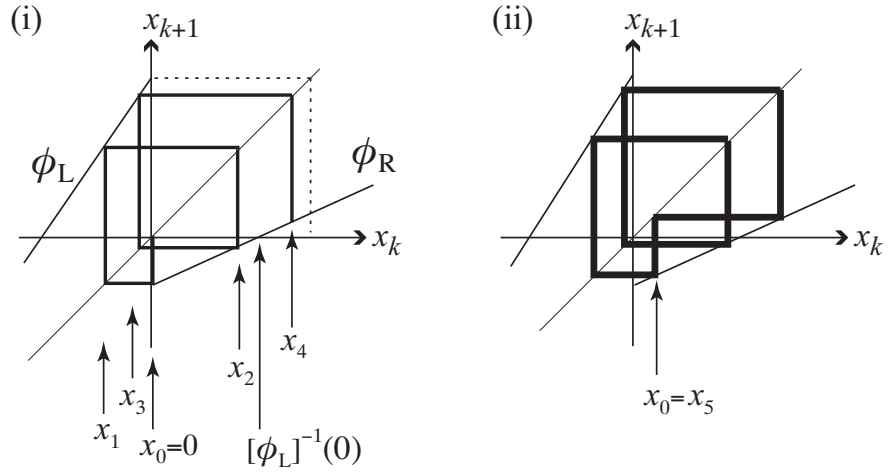

Figure 13: (i) An orbit of the form $(RL)^n R$ shown up to $n = 2$. (iii) A period $\kappa = 5$ orbit of the piecewise linear map (18), where $x_0 = x_5$ is a fixed point of the map (29).

large κ are always stable, since $|v| < 1$ by (22), so the leftthand side tends to zero as $\kappa \to \infty$. We now turn to existence conditions for such orbits.

In a period $\kappa = 2n + 1$ orbit, with $n \in \mathbb{Z}$ and containing a point (40), the first $2n$ iterates are obtained by applying the map Φ_R to $x_i \geq 0$ for all even i up to $i = 2n$, and by applying Φ_L to $x_i \leq 0$ for all odd i up to $i = 2n - 1$. Since the orbit is periodic, the last iterate must equal the first, $x_{2n+1} = x_0$, and becomes the only odd iterate with a positive sign. (For $\kappa = 5$ the sequence of iterates with $x_0 = 0$ and with a general $x_0 = x_\kappa$ are shown in figure 13). Thus we have an ascending sequence of iterates with an initial point $x_0 > 0$, the odd iterates

$$x_1 < x_3 < ... < x_{\kappa-2} < 0 \leq x_\kappa, \tag{42}$$

and the even iterates, obtained by applying to these the inverse map $[\phi_R]^{-1}$,

$$0 \leq x_0 < x_2 < ... < x_{\kappa-3} < [\phi_R]^{-1}(0) < x_{\kappa-1}, \tag{43}$$

which are given by (29), and where $[\phi_R]^{-1}(0) = -(\mu+\lambda)/v_R$. The values of μ for which such orbits can exist are found as follows.

Firstly, if $\mu_R < \mu < \mu_L$ then no such sequences, and therefore no such orbits, are possible. This is because, by (34), there exists a period two orbit with iterates $(x_L^{**}, x_R^{**}) = ((\xi - \mu)/v_L, \xi)$. These are fixed points of the second iterate maps $\Phi_{L,R}$, therefore the sequence (42) would asymptotically approach x_L^{**}, and hence could not undergo the change in sign required from $x_{\kappa-2}$ to x_κ.

For $\mu \gtrsim \mu_L$, the points $(x_L^{**}, x_R^{**}) = ((\xi - \mu)/v_L, \xi)$ are no longer fixed points of the map (18) because $x_L^{**} > 0$ by (34). Iterates of Φ_R and Φ_L are attracted monotonically towards ξ and $(\xi - \mu)/v_L$ respectively, but using (32) with (30), and taking $\mu \gtrsim \mu_L$, a little algebra shows that

$$\xi(\mu) = \frac{\lambda v_L}{1 - v}\left(1 - \frac{\mu}{\mu_R}\right) = \mu + \frac{\lambda v_L(1 - \mu/\mu_L)}{1 - v} > \mu. \tag{44}$$

therefore the attracting point ξ lies outside the invariant interval $\mathcal{I} = [\mu + \lambda, \mu]$. So iterates of Φ_R form an ascending sequence towards the boundary of $\mathcal{I}$, but the map Φ_R becomes invalid before ξ is reached, because the iterates of Φ_L undergo a change in sign as in (42), and the even iterates forming a sequence (43).

The case of $\mu < \mu_R$ yields similar, decreasing sequences

$$x_1 > x_3 > ... > x_{2n-1} > 0 \geq x_\kappa, \tag{45}$$

$$0 \geq x_0 > x_2 > ... > x_{\kappa-3} > [\phi_L]^{-1}(0) > x_{\kappa-1}, \tag{46}$$

of orbits of the form $(RL)^n L$ given by $x_{2n} = \phi_L(\phi_R \circ \phi_L)^n(x_0)$, with iterates of Φ_L attracted towards the point x_L^{**} outside $\mathcal{I}$. Corresponding results for this case are obtained by making the replacement $\{x, v_R, v_L, \mu\} \mapsto \{-x, v_L, v_R, -\mu - \lambda\}$ in the analysis for $\mu \geq \mu_L$.

The conditions for the existence of periodic orbits of the form (29) are, therefore, that the inequalities (43) are satisfied. In fact, since Φ is monotonic on the interval $\mathcal{I}$ we need only the conditions on the iterates $x_{\kappa-1}$ and $x_{\kappa-3}$ (which imply the conditions on $x_{\kappa-2}$ and x_κ simply by applying ϕ_R once), so this implies that a period κ orbit of the form (39) exists if

$$x_{\kappa-3} \ < \ [\phi_R]^{-1}(0) \ \leq \ x_{\kappa-1} \quad \text{for } \mu \gtrsim \mu_L. \tag{47}$$

Substituting in expressions for the even iterates $x_{\kappa-1}$ and $x_{\kappa-3}$ from (29), and using $x_0 = x_\kappa$ given by (40) as an initial point, one obtains explicit ranges of the parameter μ and gradients $v_{R,L}$ for which a period κ orbit can exist. The expressions obtained, however, are somewhat complicated. These bounds are illustrated in figure 14.

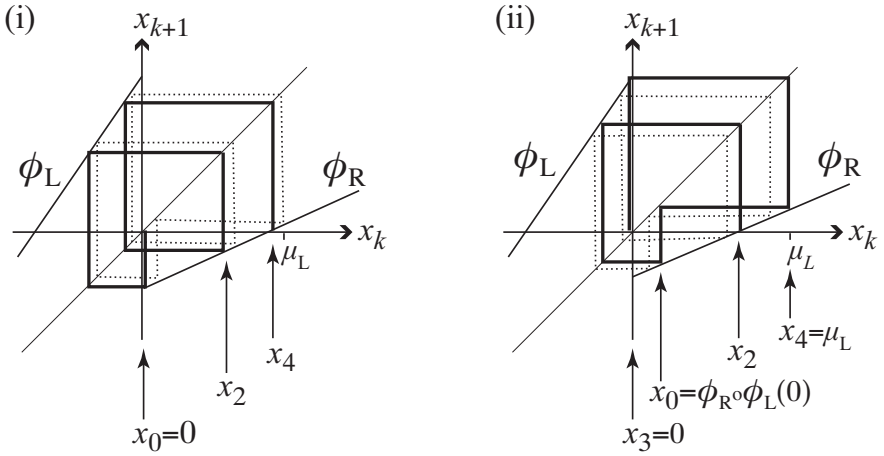

Figure 14: The range of existence of a period 5 orbit in (18), showing: (i) the orbit of the point $x_0 = 0$ and a nearby period 5 orbit, (ii) the orbit of the point $x_0 = \phi_R \circ \phi_L(0)$, and a nearby period 5 orbit (dotted) is shown in both.

This can be simplified significantly if, instead of finding x_0 by solving (40), we replace x_0 with its value in the bounding cases, when $x_{\kappa-3} = [\phi_R]^{-1}(0)$ or $[\phi_R]^{-1}(0) = x_{\kappa-1}$. Taking the left bound first, $x_{\kappa-3} = [\phi_R]^{-1}(0)$, implies that $x_0 = x_\kappa = \phi_R \circ \phi_L \circ \phi_R(x_{\kappa-3}) = \phi_R \circ \phi_L(0)$. Using (29) with $x_0 = \phi_R \circ \phi_L(0) = \lambda(1 - \mu/\mu_L)$ to express $x_{\kappa-3}$, and substituting this into (47), and recalling that $[\phi_R]^{-1}(0) = (-\mu - \lambda)/v_R$, gives

$$\lambda\left(1 - \frac{\mu}{\mu_L}\right) v^{\frac{\kappa-3}{2}} + \left(1 - \frac{\mu}{\mu_R}\right) \frac{(1 - v^{\frac{\kappa-3}{2}})}{(1-v)} \lambda v_L < \frac{-\mu - \lambda}{v_R}$$

which can be re-arranged to

$$\mu - \mu_L < \frac{\mu_L}{-\lambda} \frac{(1-v)v^{\frac{\kappa-1}{2}}}{\frac{v_L}{\mu_L} + \left(\frac{1-v}{\mu_L} - \frac{v_L}{\mu_R}\right) v^{\frac{\kappa-1}{2}}}$$

This places a lower bound on the distance $\mu - \mu_L$, from the border collision at $\mu - \mu_L$, over which a period κ orbit can form. Conversely, it places an upper limit on the period κ of an orbit that is possible for a given μ. Inverting, we obtain the upper bound on the allowed period κ at a given μ as

$$\kappa < 3 + \frac{2}{\log(1/v)} \log \frac{\left(1 - \frac{\mu}{\mu_R}\right) v + \left(1 - \frac{\mu}{\mu_L}\right)(1-v)v_R}{\left(1 - \frac{\mu}{\mu_R}\right) + \left(1 + \frac{\mu}{\lambda}\right)(1-v)}. \tag{48}$$

This expression is plotted in figure **??**.

More interesting are the upper bound on the distance $\mu - \mu_L$, and lower bound on the period κ. Taking the right bound in (47), $[\phi_R]^{-1}(0) = x_{\kappa-1}$, implies that $x_0 = x_\kappa = \phi_R(x_{\kappa-1}) = 0$. Using (29) with $x_0 = 0$ to express $x_{\kappa-1}$, substituting this into (47), and recalling that $[\phi_R]^{-1}(0) = -(\mu+\lambda)/v_R$, gives

$$\frac{-\mu - \lambda}{v_R} \leq \left(1 - \frac{\mu}{\mu_R}\right) \frac{1 - v^{\frac{\kappa-1}{2}}}{1-v} \lambda v_R,$$

which rearranges (using (30) and noting (35)) to

$$\mu - \mu_L \geq \mu_L \frac{\left(\frac{\mu_L}{\mu_R} - 1\right) v^{\frac{\kappa+1}{2}}}{1 - \frac{\mu_L}{\mu_R} v^{\frac{\kappa+1}{2}}}. \tag{49}$$

This places an upper bound on the distance $\mu - \mu_L > 0$ from the border collision for which an orbit of period κ can exist. It also places a lower bound on the period κ that is possible for a given μ, made explicit by rearranging (49) to

$$\kappa > \frac{2 \log \frac{(\mu - \mu_R)\mu_L}{(\mu - \mu_L)\mu_R}}{\log(1/v)} - 1, \tag{50}$$

written so the arguments of both logarithms are positive for $\mu > \mu_L$. This bound is plotted in figure 15 (the curves with $v_c = 0$ only). A few simple observations are immediately possible. As $\mu \to \mu_L$ with $\mu - \mu_L \geq 0$, the argument of the second logarithm tends to positive infinity, hence

$$\kappa \to \infty \qquad \text{as} \quad \mu \to \mu_L. \tag{51}$$

This implies that, as we approach the border collision, the allowed period of a periodic orbit of the form (39) increases exponentially, tending to infinity. Thus a cascade of orbits of increasing period will be seen as μ approaches the border collision. The infinite period orbit is of the form required by (20). Furthermore, by (41), we see that this orbit is stable. Letting $\kappa \to \infty$ in (49) gives the converse,

$$\mu \to \mu_L \qquad \text{as} \quad \kappa \to \infty, \tag{52}$$

meaning that an infinite period orbit of this form is possible *only* at the border collision.

The bound (49) can be used to characterise cascades observed in simulations. For large κ, condition (49) becomes

$$\mu - \mu_L \;\; \geq \;\; \mu_\kappa - \mu_L \;\; := \mu_L \left(\frac{\mu_L}{\mu_R} - 1\right) v^{\frac{\kappa+1}{2}} + \mathsf{O}\left(v^{\kappa+1}\right), \tag{53}$$

introducing a constant, μ_κ, so that a period κ may exist for $\mu \geq \mu_\kappa$. In simulations of a system of the form (18), one can measure the values μ_κ for three different periods $\kappa = a, b, c$, then eliminate the quantities μ_R and v, and solve for the parameter μ_L at which the border collision occurs. For

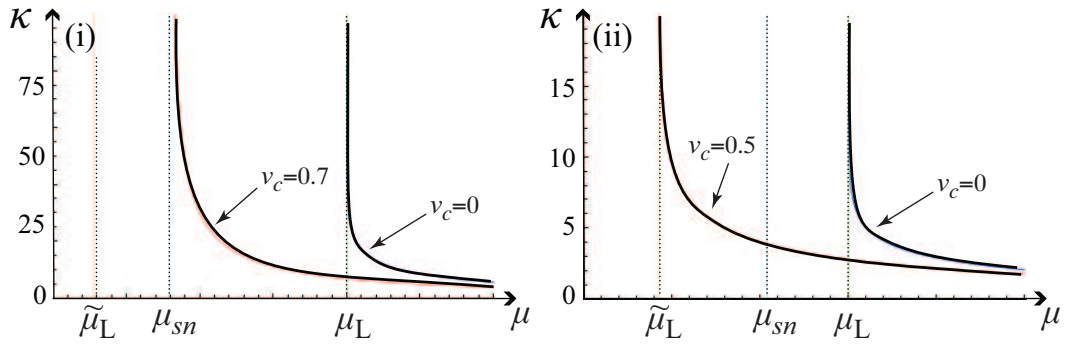

Figure 15: Smallest allowed period κ of an orbit of the form $(RL)^n R$, $\kappa = 2n+1$, showing that $\kappa \to \infty$: (i) as $\mu \to \mu_{sn}$ when $v_L = 0.8$, $v_R = 0.9$, $v_c = 0.7$; (ii) as $\mu \to \tilde{\mu}_L$ when $v_L = 0.8$, $v_R = 0.3$, $v_c = 0.5$. In both cases we also show that $\kappa \to \infty$ as $\mu \to \mu_L$ if we set $v_c = 0$. The graphs are calculated from (87); the $v_c = 0$ graphs can also be calculated from (**??**).

particular values of a, b, c, we can obtain an explicit solution for μ_L as follows. The expression for μ_κ above can be rearranged to the form

$$\frac{\mu_L}{\mu_R} - 1 = \left(\frac{\mu_\kappa}{\mu_L} - 1\right) v^{-\frac{\kappa+1}{2}} + \mathsf{O}\left(v^{\kappa+1}\right).$$

Since the lefthand side of this expression is independent of the period, the quantity on the righthand side remains fixed whatever the period κ. Therefore, one may equate the righthand side for two periods $\kappa = a, b$, then rearrange to eliminate the unknown μ_R, to find

$$v \approx \left(\frac{\mu_b - \mu_L}{\mu_a - \mu_L}\right)^{\frac{2}{b-a}},$$

which is the result (8) used in section 2. Here again, the lefthand side is independent of the period, and therefore by equating the righthand sides for two different integer pairs (a, b) and (a', b'), we can numerically solve for μ_L and v. If we choose those pairs to have the same difference, $b - a = b' - a' = 2p$ for some integer p, then we can solve explicitly to obtain

$$v \approx \frac{\mu_{a'+2p} - \mu_L}{\mu_{a'} - \mu_L} \approx \frac{\mu_{a+2p} - \mu_L}{\mu_a - \mu_L}.$$

Solving these simultaneous equations for μ_L gives

$$\mu_L \approx \frac{\mu_{a+2p}\mu_{a'} - \mu_{a'+2p}\mu_a}{\mu_{a+2p} + \mu_{a'} - \mu_{a'+2p} - \mu_a}, \tag{54}$$

which is the result (9) used in section 2. Finally, we remark that this derivation (53)-(54) can be made exact by starting from (49) instead of (53), without discarding terms of order $v^{\kappa+1}$ as we have done above, with only moderately more complication. However, when we apply this as an approximate description of higher dimensional nonlinear systems, the formulation assumes attractive orbits ($v < 1$) and small distance $\mu - \mu_L$ from the border collision (equivalently large κ), so an approximation to first order in $v^{\frac{p+1}{2}}$ is sufficient.

4.5 Border collision

The border collision described in the defining conditions (19)-(20) occurs when $\mu = \mu_L$. Setting $\mu = \mu_L$ in the expression (32) gives the iterates of the period two orbit as

$$(x_L^{**}, x_R^{**}) = \left(0,\ \frac{v_L\lambda\,(1-\mu_L/\mu_R)}{1-v}\right), \tag{55}$$

which therefore has an iterate on the discontinuity, $x = 0$, and satisfies condition (19). If we set $\mu = \mu_L$ in (40), substitute in (29) and (55), then some algebra using (30) gives the κ^{th} iterate of a period $\kappa = 2n + 1$ orbit as

$$x_\kappa(\mu_L) = \phi_R \circ \Phi_R(x_\kappa) = 0, \qquad \kappa \to \infty. \tag{56}$$

This provides the infinite period orbit with an iterate on the discontinuity required by condition (20). The period κ is infinite due to its μ-dependent lower bound from (50), and furthermore, by (41), this orbit is guaranteed to be stable.

The point $x = 0$ is initially mapped, by ϕ_L, around the period two orbit in the region $x \geq 0$, or is mapped away from it into $x < 0$ by ϕ_R. The latter of these remains in the invariant interval $\mathcal{I}$, and more specifically inside the domain of attraction of the period two orbit, and consequently it undergoes an infinite sequence of iterations, each of which crosses the discontinuity, tending asymptotically and monotonically towards the period two orbit, which eventually returns it to the discontinuity.

Thus at the border collision there exist two stable periodic orbits, one of each of them mapping from the discontinuity to $\phi_L(0) < 0$ or $\phi_R(0) > 0$. Their coexistence is allowed by the definition of the piecewise linear map (18), which permits either map $\phi_{L,R}$ to be applied at $x = 0$. That one may break the lack of uniqueness at $x = 0$ by changing the choice of inequality signs in (18) is unimportant. The results in sections 4.3-4.4 reveal the existence of a period two orbit for μ inside the region (μ_R, μ_L), and the existence of a cascade of orbits of increasing period as μ approaches μ_L from outside that region. Close to the border collision at μ_L, these orbits are guaranteed to be stable. A similar analysis gives the existence of a cascade of orbits of increasing period as μ approaches μ_R from outside (μ_R, μ_L).

4.6 Overlapping regions and Farey sequences

...

5 Nonlinear map with a gap

Let us now extend the results above by considering the effect of nonlinearity. We consider the piecewise linear map (18) to be the leading order term in a Taylor expansion about the discontinuity. To investigate the effect of adding nonlinearity, let us leave ϕ_L linear and add a higher order term to ϕ_R. Trouble is immediately encountered, since even the addition of a quadratic term, for example taking $\phi_R(x) = \mu + \lambda + v_R x + v_c x^2$ for some constant v_c, yields a map for which iterates cannot be expressed in closed form, except in special cases. Instead of approximating ϕ_R by a truncated Taylor series, we can approximate it by a rational function $P(x)/Q(x)$ where P and Q are polynomials, a general method of approximation developed by Padé and Frobenius [??r], allowing us to write $\phi_R(x) = \mu - \lambda + v_R x + v_c v_R x^2 + \mathsf{O}\left(x^3\right) = \mu - \lambda + \frac{v_R x}{1 - v_c x} + \mathsf{O}\left(x^3\right)$. Neglecting higher order terms,

we therefore study the system

$$x \mapsto \begin{cases} \phi_R(x) &= \mu - \lambda + \frac{v_R x}{1 - v_c x}, & \text{if} \quad x \geq 0, \\ \phi_L(x) &= \mu + v_L x, & \text{if} \quad x \leq 0. \end{cases} \tag{57}$$

As with the linear map, we will exclusively consider the case $\lambda < 0$, which can be scaled so that $\lambda = -1$. We assume that the new parameter, v_c, is positive, and to preserve the invariance of the interval $\mathcal{I} = [\phi_R(0), \phi_L(0)] = [\mu + \lambda, \mu]$, we fix

$$\mu v_c < 1, \tag{58}$$

then the divergence of ϕ_R at $x = 1/v_c$, which is an artifice of the rational function approximation, lies outside of $\mathcal{I}$. Note that (57) reduces to (18) for $v_c = 0$.

We will not conduct a complete analysis of the dynamics made possible by adding nonlinearity to the piecewise linear map. We confine our analysis to the effect of the perturbation v_c on the cascade analysed in the piecewise linear map in section 4.

As for the piecewise linear map we will not be concerned with fixed points of the map (57), but for completeness we note that these lie at $x = x^*_{L,R}$, and exist if and only if $x^*_L := \frac{\mu}{1 - v_L} < 0$ (stable if $|v_L| < 1$), or $x^*_R = \frac{1 - v_R \pm \sqrt{(1 - v_R)^2 - 4v_c(\mu + \lambda)}}{2v_c} > 0$ (the signs $-/+$ gives stable/unstable orbits respectively). The stable solutions coincide with the fixed points of the piecewise linear map for $v_c = 0$.

5.1 Orbits of the form RL

A period two orbit of the form RL has iterates (x_L, x_R), satisfying

$$x_L = \phi_R \circ \phi_L(x_L), \qquad x_R = \phi_L \circ \phi_R(x_R). \tag{59}$$

For the nonlinear map (57) these have two solutions, given by

$$x^\pm_L = \frac{\xi^\pm(\mu) - \mu}{v_L}, \qquad x^\pm_R = \xi^\pm(\mu) := \frac{1 - v + v_c p(\mu) \mp \theta(\mu)}{2v_c}, \tag{60}$$

in terms of the pair of functions

$$p(\mu) \;=\; \mu + v_L(\lambda + \mu) = v_L \lambda (1 - \mu/\mu_R), \tag{61}$$

$$\theta(\mu) \;=\; \sqrt{(v_c p(\mu) + 1 - v)^2 - 4v_c p(\mu)}, \tag{62}$$

and where $\sqrt{a}$ denotes the principle root $\sqrt{a} = |a|^{1/2} e^{i \arg(a)/2}$. We will again in this section make use of the parameters $\mu_{L,R}$, defined in (30).

These period two solutions exist while $x^\pm_{L,R}$ are real and $x^\pm_L \leq 0 \leq x^\pm_R$, giving existence conditions

$$\frac{\xi^\pm(\mu) - \mu}{v_L} \leq 0 \leq \xi^\pm(\mu), \tag{63}$$

$$\text{and} \qquad [\theta(\mu)]^2 > 0. \tag{64}$$

From the definition of $\xi^\pm$ in (60), it is useful to note that

$$\xi^+ \xi^- = p/v_c, \quad \text{and} \quad \xi^- - \xi^+ = \theta/v_c, \tag{65}$$

and, moreover,

$$|\xi^{\pm}|^2 = \xi^+\xi^- = p/v_c \qquad \text{if } \theta^2 < 0, \tag{66}$$

$$0 < \xi^+ < (1-v)/v_c < \xi^- < \mu < 1/v_c \qquad \text{if } \theta^2 > 0. \tag{67}$$

The first line follows simply from the definition of $\xi^{\pm}$ when θ is imaginary. In the second line, the relation of $\xi^{\pm}$ to v follows from (65) when θ is real (and therefore $\theta > 0$ by definition), the remainder following from (60) with $x_L^{\pm} < 0 < x_R^{\pm}$ and given $\mu v_c < 1$ from (58).

The stability of these orbits is determined by whether the absolute value of the derivative

$$\frac{\partial}{\partial x}[\phi_L \circ \phi_R(x_R^{\pm})] = \frac{v}{(1-v_c\xi^{\pm}(\mu))^2}$$

is smaller than unity. Using (67) we can order these derivative according to

$$\frac{v}{(1-v_c\xi^+)^2} < 1 < \frac{v}{(1-v_c\xi^-)^2}, \tag{68}$$

so that the iterates (x_L^+, x_R^+) describe a stable orbit, and (x_L^-, x_R^-) an unstable orbit. The solution (x_L^+, x_R^+) becomes the stable period two orbit (32) of the piecewise linear map (18) when $v_c = 0$. By (67), we have that the stable orbit lies to the left of the unstable orbit, that is, $x_L^+ \le x_L^-$ and $x_R^+ \le x_R^-$.

Substituting in the expressions for $\xi^{\pm}$ and θ into (63)-(64), one can obtain explicit conditions on μ for the existence of period two orbits. The algebra is fairly involved and one must check whether a given solution applies to ξ^+ or ξ^-. We are concerned only with the existence of the stable period two orbit, whose iterates are (x_L^+, x_R^+), and we find existence conditions

$$\mu_R \le \mu \le \tilde{\mu}_L \qquad \text{if} \quad \xi^+(\tilde{\mu}_L) + \xi^-(\tilde{\mu}_L) - 2\tilde{\mu}_L > 0, \tag{69}$$

$$\mu_R \le \mu \le \mu_{sn} \qquad \text{if} \quad \xi^+(\tilde{\mu}_L) + \xi^-(\tilde{\mu}_L) - 2\tilde{\mu}_L < 0, \tag{70}$$

under the assumption $|v| < 1$ from (22), and where we introduce

$$\mu_{sn} := \mu_R\left(1 - \frac{(1-\sqrt{v})^2}{v_c v_L \lambda}\right), \tag{71}$$

which is the solution of $\theta(\mu_{sn}) = 0$, and

$$\tilde{\mu}_L = \frac{\frac{1}{\mu_L} + v_c - \sqrt{\frac{4v_c}{\lambda} + \left(\frac{1}{\mu_L} + v_c\right)^2}}{-2v_c/\lambda}, \tag{72}$$

which is a solution of $\xi^+(\tilde{\mu}_L) = \tilde{\mu}_L$, for which $x_L^+ = 0$. The parameter $\tilde{\mu}_L$ becomes μ_L when $v_c = 0$. Solving $\xi^{\pm}(\mu) = \mu$ is equivalent to finding the roots of the polynomial

$$\Omega^{\pm}(\mu) = (\mu + \lambda)(1 - v_c\xi^{\pm}(\mu)) + v_R\xi^{\pm}(\mu), \tag{73}$$

when $\xi^+(\mu) = \mu$. The function $\Omega^{\pm}$ will be of further use later.

5.2 Orbits of the form $(RL)^n R$

Considering the nonlinear map as a perturbation of the piecewise linear map (18), we now follow similar analysis to section 4.4. There it was shown that, in the absence of period two orbits, there is a lower bound for the allowed period $\kappa = 2n+1$ of orbits of the form $(RL)^n R$, given by

$$x_{2n+1} = \phi_R \circ (\phi_L \circ \phi_R)^n(x_0),$$

and satisfying (20) at the border collision. This bound was arrived at from the condition (47), that is, by considering the condition

$$[\phi_R]^{-1}(0) \leq x_{\kappa-1}.$$

As in section 4.4, to evaluate $x_{\kappa-1}$ for $\kappa = 2n+1$ odd, we require an expression for $x_{\kappa-1} = x_{2n} = (\phi_L \circ \phi_R)^n(x_0)$. We begin with the second iterate map on the region $x \geq 0$,

$$x_{i+2} = \Phi_R(x_i) = \phi_L \circ \phi_R(x_i) = p(\mu) + \frac{v x_{i-2}}{1 - v_c x_{i-2}}, \tag{74}$$

where p was defined in (62). To solve for x_i in terms of x_0, let

$$x = \frac{\alpha}{\beta}, \tag{75}$$

which fixes α and β up to a relative scaling. Substituting these into (74), they are found to obey the bilinear map

$$\frac{\alpha_i}{\beta_i} = \frac{(v - v_c p)\alpha_{i-2} + p\beta_{i-2}}{\beta_{i-2} - v_c \alpha_{i-2}}, \tag{76}$$

which is exactly solvable, and implies that α and β obey

$$\begin{pmatrix} \alpha_i \\ \beta_i \end{pmatrix} = W(\mu) \begin{pmatrix} \alpha_{i-2} \\ \beta_{i-2} \end{pmatrix}, \tag{77}$$

where

$$W(\mu) = \begin{pmatrix} v - v_c p(\mu) & p(\mu) \\ -v_c & 1 \end{pmatrix}. \tag{78}$$

The real 2×2 matrix W can be decomposed into (omitting arguments)

$$W = \omega^+ W^+ + \omega^- W^-,$$

where $W^\pm$ are fixed by the conditions

$$W^\pm W^\pm = W^\pm \qquad \text{and} \qquad W^\pm W^\mp = 0,$$

which give

$$W^\pm = \pm \frac{v_c}{\theta} \begin{pmatrix} -\xi^\pm & p/v_c \\ -1 & \xi^\mp \end{pmatrix}, \tag{79}$$

then $\omega^\pm$ are the eigenvalues of W, given by

$$\omega^\pm = 1 - v_c \xi^\pm, \tag{80}$$

in terms of the functions $\xi^{\pm}$ defined in (60). The solution to (77), letting $i = 2n$ and defining an initial point $x_0 = \alpha_0/\beta_0$, is then

$$\begin{pmatrix} \alpha_{2n} \\ \beta_{2n} \end{pmatrix} = W^n \begin{pmatrix} \alpha_0 \\ \beta_0 \end{pmatrix} = \left\{ (\omega^+)^n W^+ + (\omega^-)^n W^- \right\} \begin{pmatrix} \alpha_0 \\ \beta_0 \end{pmatrix}. \tag{81}$$

Taking the ratio $x_{2n} = \alpha_{2n}/\beta_{2n}$ gives the n^{th} term of the second iterate map as

$$\begin{aligned} x_{2n} &= (\Phi_R)^n(x_0) \\ &= \frac{\left\{ (\frac{\omega^-}{\omega^+})^n \xi^- - \xi^+ \right\} x_0 + \left\{ 1 - (\frac{\omega^-}{\omega^+})^n \right\} p/v_c}{\left\{ (\frac{\omega^-}{\omega^+})^n - 1 \right\} x_0 + \left\{ \xi^- - (\frac{\omega^-}{\omega^+})^n \xi^+ \right\}}, \end{aligned} \tag{82}$$

where $n \geq 1$ is an integer. For $v_c = 0$, (82) reduces to equation (29) for $x_0 \geq 0$. When the functions $\omega^{\pm}$ are real, then by (60) θ is real, so we can apply (67) to show that $|\omega^-/\omega^+| = |(1 - v_c\xi^-)/(1 - v_c\xi^+)| < 1$. Then using the identity $\xi^+\xi^- = p/v_c$ from (65), we find that (82) obeys

$$x_{2n} \to \xi^+ \quad \text{as } n \to \infty. \tag{83}$$

Thus the second iterate map (82) tends towards the point $x = \xi^+$. This corresponds to similar behaviour in the piecewise linear map, from which we recall that the second iterate map tends towards the period two orbit if it exists, and otherwise will never reach ξ^+, reaching the boundary of the invariant interval $\mathcal{I}$ first. In the case when θ is imaginary, no real limit of x_{2n} exists.

Following section 4.4, we now use this result to place a bound on the values of μ at which an orbit of odd period κ can exist, now with $v_c \neq 0$. In section 4.4, it was shown that the conditions that must be satisfied for an orbit of odd period κ to exist are

$$\phi_R(x_{\kappa-1}) \geq 0 \quad \text{given} \quad x_0 = 0, \tag{84}$$

and

$$\phi_R(x_{\kappa-3}) \leq 0 \quad \text{given} \quad x_0 = \phi_R \circ \phi_L(0). \tag{85}$$

Here we will calculate only the former of these. Substituting $x_0 = 0$ into (82) gives

$$\begin{aligned} \phi_R(x_{2n}) &= \mu + \lambda + \frac{v_R p/v_c}{\frac{\xi^- - (\frac{\omega^-}{\omega^+})^n \xi^+}{1 - (\frac{\omega^-}{\omega^+})^n} - p} \\ &= \mu + \lambda + \frac{v_R}{\frac{(1-v_c\xi^+)^n/\xi^+ - (1-v_c\xi^-)^n/\xi^-}{(1-v_c\xi^+)^n - (1-v_c\xi^-)^n} - v_c}. \end{aligned} \tag{86}$$

This should be real-valued, and while all other terms are strictly real, $\xi^{\pm}$ are complex when θ is imaginary. The potentially problematic term is

$$\frac{(1 - v_c\xi^+)^n/\xi^+ - (1 - v_c\xi^-)^n/\xi^-}{(1 - v_c\xi^+)^n - (1 - v_c\xi^-)^n}$$

in the denominator of (86), which can be expanded exactly as a polynomial in θ, and becomes, after some cancellation,

$$\frac{2v_c(1 + v - v_c p)}{(1 - v + v_c p)^2 - \theta^2} \left(\frac{1 - v + v_c p}{1 + v - v_c p} + \frac{\sum_{j=0}^{n} \binom{n}{2j} (1 + v - v_c p)^{n-2j} \theta^{2j}}{\sum_{j=0}^{n} \binom{n}{2j+1} (1 + v - v_c p)^{n-2j} \theta^{2j}} \right),$$

where $\binom{n}{2j}$ and $\binom{n}{2j+1}$ denote binomial coefficients. This quantity is then clearly real-valued since θ appears only as θ^2, which is always real.

Substituting (86) into the condition (84) and setting $\kappa = 2n+1$, we have that period κ orbits satisfy

$$\kappa \geq 1 + 2\frac{\log\left(\frac{\xi^+(\mu)\Omega^-(\mu)}{\sqrt{\xi^-(\mu)\xi^+(\mu)\Omega^-(\mu)\Omega^+(\mu)}}\right)}{\log\left(\frac{\omega^+(\mu)}{\sqrt{\omega^-(\mu)\omega^+(\mu)}}\right)}, \tag{87}$$

where $\xi^\pm$ and $\Omega^\pm$ were defined in (60), (80), and (73) respectively. This bound is plotted in figure 15. The expression (87) written in this form gives the correct phases inside the logarithms when $\xi^\pm$, $\omega^\pm$, and $\Omega^\pm$, are complex.

For $\theta^2 > 0$, all of the quantities in (87) are real, but the lower bound placed on κ is not larger than one. This is because we can use (67) to show that $(1 - v_c\xi^+)/(1 - v_c\xi^-) > 1$, therefore the denominator in (87) is positive, but $\xi^+/\xi^- < 1$ from (67), and $\Omega^-/\Omega^+ < 1$ since

$$\begin{aligned}
\Omega^+ &= (\mu+\lambda)(1 - v_c\xi^+) + v_R\xi^- \\
&= (\mu+\lambda)(1 - v_c\xi^+) + v_R(\xi^- - \theta/v_c) \\
&> (\mu+\lambda)(1 - v_c\xi^-) + v_R\xi^- = \Omega^-,
\end{aligned}$$

therefore the numerator in (87) is negative, so the righthand side of (87) cannot exceed one. The bound in such a case is shown in figure 15(ii), for v_c both zero and non-zero.

For $\theta^2 < 0$, the righthand side of (87) is real because ξ^+ and ξ^- are complex conjugates, therefore each of the ratios appearing inside the logarithms have unit length in the complex plane, the logarithms of which yield imaginary values, and the ratio of these cancels to give a real value overall. Figure 15(i) (the $v_c \neq 0$ only) shows the positive bound on κ that this imposes for $\mu \gtrsim \mu_{sn}$.

5.3 Disappearance of the period two orbit

A stable period two orbit exists for μ values satisfying the conditions (69) and (70). At the boundary of (69), the period two orbit disappears via a border collision, as we discuss in section 5.3.1 below. Introducing nonlinear terms to the map creates a new situation by which the period two orbit can disappear in a saddle-node bifurcation, which occurs at the boundary of (70) as we discuss in section 5.3.2 below. Both scenarios lead to similar bifurcation cascades, with one vital difference, discussed in sections 5.3.1-5.3.2.

If the bounds in (69) and (70) both achieve equality, that is, if $\mu = \tilde{\mu}_L = \mu_{sn}$, then a codimension two bifurcation occurs, namely a simultaneous border collision and saddle-node bifurcation. Such higher codimension events are beyond the scope of the present paper.

5.3.1 Border collision

To consider border collision of periodic orbits we assume that (69) holds. Then a stable period two orbit exists for $\mu_R \leq \mu \leq \tilde{\mu}_L$, and has an iterate on the discontinuity when $x_L^+ = 0$ or $x_R^+ = 0$. The latter case was omitted from section 4.3, because it could be derived from the former by a straightforward transformation, and again we omit it here.

The border collision of a stable period two orbit for which $x_L^+ = 0$ occurs when $\mu = \tilde{\mu}_L$, defined in (72). Since $\tilde{\mu}_L$ becomes μ_L when $v_c = 0$, this corresponds to a perturbation of the border collision at $\mu = \mu_L$ considered for the piecewise linear map in section 4.

For $\mu \gtrsim \tilde{\mu}_L$ the stable period two orbit no longer exists. In this region, instead, from section 5.2, we have orbits of the form $(RL)^n R$, whose period κ is bounded below by (87). We must now consider the limit of this bound as $\mu \to \tilde{\mu}_L$, which depends on the behaviour of $\xi^{\pm}(\mu)$ and $\Omega^{\pm}(\mu)$. By the definition of $\Omega^{\pm}$ from (73) we have $\Omega^+(\tilde{\mu}_L) = 0$, and therefore

$$\log\left(\Omega^-/\Omega^-\right) \to \infty \quad \text{as } \mu - \tilde{\mu}_L \to 0^+. \tag{88}$$

Since $(1 - v_c\xi^+)/(1 - v_c\xi^-) \geq 1$ by (67), the denominator in (87) is positive, and so

$$\kappa \to \infty \quad \text{as } \mu - \tilde{\mu}_L \to 0^+. \tag{89}$$

Therefore, as $\mu \to \tilde{\mu}_L$ from $\mu \geq \tilde{\mu}_L$, we have a cascade of orbits whose period κ increases towards infinity, as shown in figure 15(ii). This corresponds to the cascade approaching border collision in the piecewise linear map in section 4.

5.3.2 Saddle-node bifurcation

A saddle-node bifurcation occurs when the stable and unstable period two orbits coincide. That is, for $\mu < \mu_{sn}$ by (70), there exist stable and unstable period two orbits with iterates (x_L^+, x_R^+) and (x_L^-, x_R^-) respectively, as given by (60). When $\mu = \mu_{sn}$ these two solutions coincide. Note that the right iterate $x_R^{\pm} = \xi^{\pm}(\mu_{sn})$ of the saddle-node bifurcation is confined to the region $x < 1/v_c$, and therefore does not cross the divergence in the ϕ_R map at $x = 1/v_c$. (There exists a second saddle-node solution, given by changing the sign in front of the square root in (71), and this solution does cross the divergence, having its right iterate at $x_R = \frac{1+\sqrt{v}}{v_c} > \frac{1}{v_c}$; we omit this scenario here).

For $\mu \gtrsim \mu_{sn}$ we have $\theta^2 \leq 0$, and the period two orbits no longer exist. Instead, from section 5.2, there exist orbits of the form $(RL)^n R$, whose period κ is bounded below by (87), which for θ imaginary becomes

$$\kappa \geq 1 + 2\frac{\log\left(\frac{\xi^+(\mu)\Omega^-(\mu)}{\xi^-(\mu)\Omega^+(\mu)}\right)}{\log\left(\frac{1-v_c\xi^+(\mu)}{1-v_c\xi^-(\mu)}\right)} = 1 + 2\frac{\arg\xi^+ + \arg\Omega^-}{\arg(1 - v_c\xi^+)}.$$

All three of these arguments tend to zero as μ tends to μ_{sn}, so the relative rate at which they do so determines the bound on κ. We have

$$\begin{array}{lll} |\arg\xi^+| & = \arctan\frac{\theta}{1-v+v_cp} & \approx \arctan\frac{\theta}{1-v}, \\ |\arg(1-v_c\xi^+)| & = \arctan\frac{\theta}{1+v-v_cp} & \approx \arctan\frac{\theta}{1+v}, \\ |\arg\Omega^-| & = \arctan\dfrac{\theta}{1+\frac{\frac{v_R}{v_c}+\mu+\lambda}{\frac{v_R}{v_c}-\mu-\lambda}(v_cp-v)} & \approx \arctan\frac{\theta}{1-v}, \end{array}$$

approximating for small v_c, which gives $|\arg(1 - v_c\xi^+)| < |\arg\xi^+|$ and $|\arg(1 - v_c\xi^+)| < |\arg\Omega^-|$, so the denominator of (87) tends to zero faster than the numerator, giving

$$\kappa \to \infty \quad \text{as } \mu - \mu_{sn} \to 0^+. \tag{90}$$

Such limiting behaviour is shown in figure 15(i) ($v_c \neq 0$ curve only). This result holds more generally than for small v_c, however, for brevity, we omit further investigation here. We therefore have that, just as a cascade occurs as μ approaches the appearance of a stable period two orbit in a border collision at $\mu = \tilde{\mu}_L$, a cascade occurs similarly as μ approaches the appearance of a stable period two orbit in a saddle-node bifurcation at $\mu = \mu_{sn}$.

6 Concluding remarks

Grazing of a period two orbit creates an infinite period attractor that itself grazes. The saddle-node bifurcation liberates the infinite period attractor from grazing...

The cascades of section 4 and section 5 appear to account well for those observed in the cell cycles models of section 2, and this was verified quantitatively by calculating the location of a border collision in the nine dimensional model. It is quite remarkable that the phenomenon is sufficiently robust to survive from fundamental origins in a one-dimensional map, to observation in highly nonlinear four and nine dimensional biological models. Lest this outcome be overestimated, however, we must discuss the various other behaviours that are observed in the cell cycle model.

For the four dimensional model, considering only the scalar map of m works particularly well, because u_1, u_2, u_3, are almost constant on $u_1 = 0$ for $\dot{u}_1 > 0$ throughout the different cycles of a periodic orbit. This is not so in the nine dimensional model. Though this evidently does not destroy the applicability of the cascade scaling, it does make it easier for variations in the various u_i to allow more complex periodic orbits to form, and the cascades associated with them are consequently more complex. For example, by slightly decreasing r in the cascade reported above, one observes a cascade triggered by grazing of an orbit of period four, rather than two. Period four orbits do not occur in a one dimensional map of the local form (57), hence this reveals the multi-dimensionality of the full system changing the qualitative form of the cascade. Nevertheless, a cascade does occur, and in a similar manner, though a sequence of odd periods which, however, does not visit all odd integers. Further analysis of such scenarios will require the study of two-dimensional maps with gaps.

Changing the value of r further, one finds that orbits may make many loops between cell divisions, whereas in section 2 we observed only one loop. The result is that any of these loops may graze the discontinuity surface, leading to many discontinuities in any global return map, which could be called a "map with many gaps". One could consider a scalar map of the form $\phi(x) = \phi_r(x)$, where each ϕ_r is a smooth function over a region $x_{r-1} < x < x_r$, and where $\phi_{r-1}(x_{r-1}) > \phi_r(x_{r-1})$. This represents a flow in which different periods consist of different numbers, r, of loops, each of which increases the length of that period. Cascades can occur as in sections 4-5, accumulating either at a grazing of a period two orbit, or at a saddle-node bifurcation. When the period two orbit with iterates on the r_1 and r_2 branches vanishes, the system can map around the intervening branches $r_1 < r < r_2$. Provided a generalization of the conditions given in section 4.1, that the period two orbit lies in an invariant region that includes the $r_2 - r_1$ discontinuities, then after sufficient iterations any orbit should return to the r_1 and r_2 branches, after which the analysis in this paper can be applied to place a lower bound on the number of iterations required to form a new periodic orbit. Hence cascades may be expected to occur, but their precise form will depend on closer analysis.

Although we began, in (20), by assuming the existence of an infinite period orbit homoclinic to the discontinuity, the conditions under which this occurs are quite general, and in those cases, seems to be an inevitable consequence of the disappearance of a period two orbit via grazing or saddle-node bifurcation. Intuitively, when a stable period two orbit vanishes, the system strives towards the vanished orbit over an even number iterates $2n$, then is interrupted by the discontinuity, adding one iterate that re-injects the orbit back towards its starting point; a periodic orbit of this form then has period $2n + 1$.

Most interesting perhaps is the more general question brought up by the cascade, namely the behaviour of the mirage attractor or this attraction-to-grazing...